HYDRODYNAMICS AT PELLESTRINA (VENICE)

Written by Marcello Di Risio
Under the supervision of Giorgio Bellotti and Leopoldo Franco

TABLE OF CONTENTS:

LIST OF FIGURES:

1. Summary

The aim of this work is to investigate the nearshore circulation induced by breaking waves at Pellestrina beach(Venice). In the tests presented here monochromatic ideal waves and two types of bathymetric configurations were considered: an ideal beach and a real beach (based on March 1999 survey). Computing is based on uncoupled approach. The wave height and propagation direction were computed by a parabolic numerical model. Then the wave driving force was computed from the values of the radiation stress components. These values were then introduced (given as input to) in a 2DH nearshore circulation model based on the non-linear shallow water equations (see equations 2.1-2.2-2.3).

2. Nearshore circulation numerical model

The 2DH numerical model utilized here is based, as stated before, on the non linear shallow water equations. The 2DH numerical model used here is based on the Nonlinear Shallow Water Equations (NSWE) which read:

$$\frac{\partial z}{\partial t} = -\frac{\partial}{\partial x}\left[U(h+z)\right] - \frac{\partial}{\partial y}\left[V(h+z)\right] \tag{2.1}$$

$$\frac{\partial U}{\partial t} = -U\frac{\partial U}{\partial x} - V\frac{\partial U}{\partial y} - g\frac{\partial z}{\partial x} - \frac{1}{\rho(z+h)}\left[\left(\frac{\partial S^{w}_{xx}}{\partial x} + \frac{\partial S^{w}_{yx}}{\partial y}\right) + \left(\frac{\partial S^{t}_{xx}}{\partial x} + \frac{\partial S^{t}_{yx}}{\partial y}\right)\right] - \frac{\tau^{B}_{x}}{\rho(z+h)} \tag{2.2}$$

$$\frac{\partial V}{\partial t} = -U\frac{\partial V}{\partial x} - V\frac{\partial V}{\partial y} - g\frac{\partial z}{\partial y} - \frac{1}{\rho(z+h)}\left[\left(\frac{\partial S^{w}_{xy}}{\partial x} + \frac{\partial S^{w}_{yy}}{\partial y}\right) + \left(\frac{\partial S^{t}_{xy}}{\partial x} + \frac{\partial S^{t}_{yy}}{\partial y}\right)\right] - \frac{\tau^{B}_{y}}{\rho(z+h)} \tag{2.3}$$

The NSWE are a hyperbolic system of partial differential equations in which it is possible to recognize the continuity equation (2.1) and horizontal momentum equations (2.2) and (2.3). The solution is constituted by the vector of **z**, **U** and **V** that respectively represent the mean water level (**z**), the x-axis component (**U**) and the y-axis component of the mean horizontal velocity.

The governing equations are solved on a regular grid by means of a finite difference method. More specifically a high order scheme for spatial derivatives and the Adam-Bashfort-Moulton predictor-corrector for time integration are used.

In the equation (2.2) and (2.3), the terms in square brackets represent the driving forces due to breaking short waves and turbulent mixing. The last term represents the shear stress on the bottom.

3. Ideal beach

3.1. Computational domain

The domain of interest was modeled to investigate the hydrodynamics processes with a very regular bottom (parallel contours). The depth distribution was derived from the real configuration of the sea bottom of cell 9 of the Lido of Pellestrina. As known, in this site the defence structure system is constituted by several groynes partially submerged that

reach a submerged breakwater parallel to the shore (with crest level at -1.5 m below mean water level).

Some information from this real beach was maintained into the ideal beach schematization:

- shoreline position;
- submerged breakwater distance from shoreline;
- groynes position;
- level of submerged breakwater crest;
- offshore depth;
- depth of submerged breakwater toe at the shore side;
- mean beach slope.

From these *fixed points* it was possible to define a regular bathymetry that in the following is referred to as the *ideal beach* (see fig. 1).

This domain type is good to investigate qualitatively the hydrodynamics phenomena occurring in a typical Pellestrina cell (with the configuration of the defence structures).

3.2. Numerical simulations

With the domain described above three tests were carried out (see tab. I), which were finalized to evaluate the effect of changing the wave direction angle. The wave height value was chosen to take in evidence the submerged breakwater effects (given its crest level). The angle of propagation direction shown in table I is referred to the x-axis direction perpendicular to the shore and point to the inshore zone with origin in the offshore one. Consequently the y-axis is directed in the longshore direction (see fig. 2)

Test	***H (m)***	***T (s)***	***Direction***
A	2.0	6.0	0°
B	2.0	6.0	10°
C	2.0	6.0	30°

Table I: Wave conditions

With regards to tab. I it is possible to understand that the study, at this step, was directed to investigate the effects of an orthogonal wave and of two oblique wave attacks. The chosen wave height allows to observe the breaking phenomena due to the presence of the submerged structure. For the oblique waves a longshore current is expected near the breakwater. The results of the wave propagation numerical model and the nearshore circulation numerical model are presented in the following.

3.3. Test A

3.3.1. Wave field

The wave height distribution computed by the adopted numerical model (see fig. 3) shows the breaking phenomena, as expected, near the submerged breakwater. The wave energy transmitted behind this structure is dissipated near the shoreline where further breaking phenomena exist. Regarding the wave height distribution the shoaling and breaking phenomena are very clearly identifiable. The refraction and diffraction phenomena can be observed from the plot of the instantaneous surface displacement from the mean water level (see fig. 4), namely a snapshot of the free surface position.

3.3.2. Nearshore circulation

The numerical model provides the values of the mean water level (its displacement from still water level) and of the mean velocity.
The mean water level (see fig. 5) computed for this test shows the presence of the set-down (about 5 cm) near the submerged breakwater due to breaking phenomena in this area. Near the shoreline a set-up can be observed (about 30 cm). The boundary condition used by the numerical model at the shoreward side simulates the presence of a wall in correspondence of a fixed depth (here 20 cm), hence shoreline is fixed in time.
With regard to the velocity pattern (see fig. 6 and fig. 7) it is possible to observe the rip current occurring between the two groynes. Near the submerged breakwater, close to the groynes head, the velocity intensity is largest (about 0.6 m/s) and here it is possible to recognize the source of rip current occurring in the middle of the cell(about 0.2 m/s). The difference of the velocity intensity (about 0.4 m/s) in these two zones is explainable by observing the width of the zone interested by the rip current (about 100 m) and the one interested by the incoming current close to the groyne (about 20 m each groyne).

The rip current presence is due to the mean water level gradient in longshore direction (the third term in right hand side of the momentum equation in the y-direction). Hence it is possible to say that this current is due to the bathymetric configuration inducing a breaking line position which varies in longshore direction with a variable distance from the shoreline.

3.4. Test B

3.4.1 Wave field

As for test A, it is possible to recognize the breaking phenomena near the submerged breakwater (see fig. 8). Also in this test the diffraction and refraction phenome na are evident. Close to the left groyne it is possible to observe the diffraction phenomena effects noting a *shadow zone* not present in the wave height distribution for orthogonal wave propagation direction (test A). The refraction phenomena (see fig. 9) are more clearly observable with reference to the instantaneous surface displacement from still water level.

3.4.2. Nearshore circulation

The computed mean water level (see fig.10) denotes some difference with respect to the test A one. First of all, the set-up value is a little bit smaller (about 27 cm) with a not symmetric pattern. This distribution is due to wave angle propagation not equal to zero

(see tab. I) by which the driving force due to wave propagation has two components: the x-component that induces the set-up and set-down and the y-component that induces a longshore current. It is important to underline that the set-down value (about 5 cm) is the same of test A because the wave energy ratio dissipated for the presence of submerged breakwater is equal.

With regards to the velocity pattern (see fig.11 and fig.12) two longshore currents are clearly observable. This phenomenon is due, as said before, to the oblique wave. The longshore current near the submerged breakwater is due to wave breaking in this zone, while the longshore current near the shoreline is due to the breaking phenomena of the wave transmitted behind the structure.

The intensities of these two currents are different, the offshore one is about 0.6 m/s and the inshore one is about 0.4 m/s. Also it is possible to observe the absence of the rip current that is degenerated to an eddy near the right groyne.

3.5. Test C

3.5.1. Wave field

Also in this test, as in previous ones, it is possible to recognize the breaking phenomena near the submerged breakwater (see fig. 13-14). Diffraction phenomena are more important in this wave condition and it is clearly observable a shadow zone close to the left groyne larger than the test B one.

3.5.2. Nearshore circulation

The results of this test denote a more important asymmetry due to a larger angle of wave propagation. The mean water level (see fig. 15), because of the minor importance of x-component of driving force, presents a set-up of about 23 cm (less than tests A and B ones). The set-down is about 5 cm as for the other tests because, as said before (see section 3.4.2), the wave energy ratio dissipated by the presence of submerged breakwater is the same.

For the velocity pattern (see fig. 16 and fig. 17) it is possible to observe that the cross-shore component of the mean velocity vector is everywhere very small (not so only close to the groynes where the longshore current goes around the structures). This can be explained because the wave propagation angle is large, consequently the y-component driving force is more important than the x-component. This is clearer regarding the intensity of the longshore current (about 1 m/s) which is larger than intest B.

3.6. Conclusions

From the tests presented above it is possible to understand the phenomena occurring with a regular bathymetric configuration similar to the cells of Pellestrina. With orthogonal wave attack a rip current takes place; this phenomenon progressively vanishes with increasing of the wave angle propagation. In fact, in test B the rip current vanishes, substituted by an eddy near the groynes. This eddy can be interpreted as a rip current transported by the longshore current that remains trapped close to the groyne. In test C the longshore current is so strong that no cross-shore velocity component is present. These phenomena can be graphically presented with the vorticity distribution in the three tests. It

is clearly observable the rip current presence for test A, the presence of the eddy near the groyne for test B and the absence of cross-shore velocity component for test C with no eddies in all the domain (see fig. 18, fig. 19 and fig. 20).

4. Real beach

4.1. Computational domain

At this step of the work, it is necessary to analyse the real beach to compare the results obtained for the ideal configuration. The survey of March 1999 data is considered and a domain of propagation was defined (see fig. 21).

4.2. Numerical simulations

The tests carried out with the real beach are similar to the ones presented above for the so that the wave break ideal beach. The wave height is chosen to verify the breaking phenomena close to the submerged breakwater and the wave angle propagation is varying from 0° (orthogonal wave) to 20° with respect to x axis (see fig. 2 and tab. II).

Test	*H (m)*	*T (s)*	*T*
D	2.0	5.0	0°
E	2.0	5.0	5°
F	2.0	5.0	10°
G	2.0	5.0	20°

Table II: Wave conditions for real bathymetry

4.3. Test D

4.3.1. Wave field

The computed wave height (see fig. 22) presents, as expected, a very irregular distribution. Even though it is possible to recognize the breaking phenomena close to the submerged breakwater and near the shoreline. Also refraction and diffraction are clearly recognizable in the instantaneous surface displacement from still level water plots (see fig. 23).

4.3.2 Nearshore circulation

The nearshore circulation numerical model provides values of the mean water level not too different from the ideal test ones (see fig. 24). In this test it is possible to appreciate an asymmetry with respect to an axis parallel to the x one, but the value of set-up (about 30 cm) and set-down (about 5 cm) are very near to those obtained above for ideal beach.

Regarding to the velocity pattern (see fig. 25 and fig. 26) it is possible to recognize the rip current, but it is not so evident as in the ideal case as it is surrounded in a system of eddies. These eddies are probably due to the irregularity of the beach (and of the submerged breakwater geometry).

These two tests are presented together because they are similar and can be commented in the same way.

4.4. Tests E and F

4.4.1 Wave field

In these two tests it is possible, as for the previous ones, to recognize where wave breaking occurs (see fig. 27 and fig. 32). Also, because the wave propagation angle is not equal to zero, there are clearly present the diffraction and refraction phenomena with reference to the instantaneous surface displacement from the still level water (see fig.28 and fig. 33)

4.4.2 Nearshore circulation

The mean water level level distributions (see fig. 29 and fig. 34) denote a higher asymmetric feature with respect to the test D with a set-up of about 30 cm and a set-down of about 5 cm. These values are the same of test D ones because the wave angle direction is very small (5° and 10°).

With regard to the velocity pattern (see fig.30 and fig. 35) it is possible to recognize the evolution of hydrodynamics phenomena presented in test B. The longshore current transports the rip current and it degenerates to an eddy close to the groyne (the right one). Also, in these real cases, there are other eddies close to the submerged breakwater due to the irregularity of the survey.

4.6. Test G

4.6.1 Wave field

This test can be commented with reference to the relative ideal case (test C). Regarding to wave field it is possible to recognize all the phenomena underlined in the tests above (shoaling, refraction and diffraction – see fig. 37 and fig. 38).

4.6.2. Nearshore circulation

As for test C, the mean water level presents a more important asymmetry due to a larger angle of wave propagation. The mean water level (see fig. 39) presents a set-up of about 30 cm and a set-down of about 5 cm.

For the velocity pattern (see fig. 40) it is possible to recognize two longshore current systems: a longshore current close to the submerged breakwater and the other one close to shoreline. Also it is clearly visible the eddy close to the groyne on the right trapped by the longshore current near the shoreline. As for the ideal test, also here the two longshore currents are of different intensity (see fig. 37) with the offshore one about 1.2 m/s and the other one about 0.6 m/s.

4.7. Conclusions

Also in this real morphological case (with monochromatic unidirectional ideal waves) it is possible to recognize a specific evolution of hydrodynamics phenomena that confirms the comment of the ideal tests. The rip current vanishes substituted by an eddy near the groyne. It is also clear that for wave angle propagation of 20° the eddy close to the groyne is still present. With irregular bottom other eddies occur, especially for small values of wave angle propagation, whilst for larger values of wave angle only a strong longshore current is present. Also in this case it is possible to appreciate the hydrodynamics phenomena evolution regarding the vorticity distribution over the domain.

5. Conclusions

In this work the nearshore currents induced by breaking waves at Pellestrina beach were studied by means of a wave-averaged numerical model.

More specifically, the typical hydrodynamics of a cell was simulated. This study was divided in two parts. In the first one a simple idealized bathymetry was used, in order to investigate the dominant characters of nearshore currents; in the second part the actualbathymetric survey of March 1999 was used to obtain a realistic computational grid. The results obtained in the two cases are similar and clearly indicate that if waves attack the coast orthogonally a rip current is induced in the middle of the cell. As wave direction deviates from the orthogonal to the coast, the longshore current becomes dominant and tends to push the rip current system towards the groynes. This general pattern seems to be valid for the actual geometrical scheme of Pellestrina (i.e. cell size of 250m x 500m) and incident wave conditions tested (H=2.0m, T=6s).

References

Baquerizo, A., Losada, M. A., Ortega, J. L. (2002), "Rip currents in semielliptic bays", *Proc. 28th Int. Conf. Coastal Engrg., ASCE*, Cardiff, Vol. 1, 718-726

Berkhoff, J.C.W. (1972), "Computation of combined refraction-diffraction", *Proc. 13th Int. Conf. Coastal Engrg., ASCE*, 471-490.

Cavaleri, L. (2000). "The oceanographic tower Acqua Alta — activity and prediction of sea states at Venice." *Coastal Eng*. 39 2000 29–70.

Di Risio, M., Archetti, R., Bellotti, G., Soldati, M. (2003). "Nearshore waves and currents at Pellestrina." *Accepted at the 6th international Conference on Mediterranean Coastal, Ravenna*

Kirby, J.T., Dalrymple, R.A. (1983). "A parabolic equation for the combined refraction-diffraction of Stokes waves by mildly varying topography", J. Fluid Mech., 136, 543-566.

Kirby, J.T., Dalrymple R.A. (1994), "Combined refraction/diffraction model REF/DIF1, Version 2.5", *Res. Report CACR-94-22, Center for Applied Coastal Research, University of Delaware.*

Radder, A.C. (1979), "On the parabolic equation method for water-wave propagation", *J. Fluid Mech.*, 95, 159-176.

Svendsen, Ib A., Haas K., Zhao Q. (2000), "Analysys of rip current system", *27th International Conference on Coastal Engineering*, Sidney, Vol. 2, 1127-1140

Van Dongeren, A.R., Sancho, F.E., Svendsen I.A., Putrevu U. (1994), "SHORECIRC: a quasi 3-D nearshore model", 24th *International Conference on Coastal Engineering, ASCE*, Kobe, Vol. 3, 2741-2754

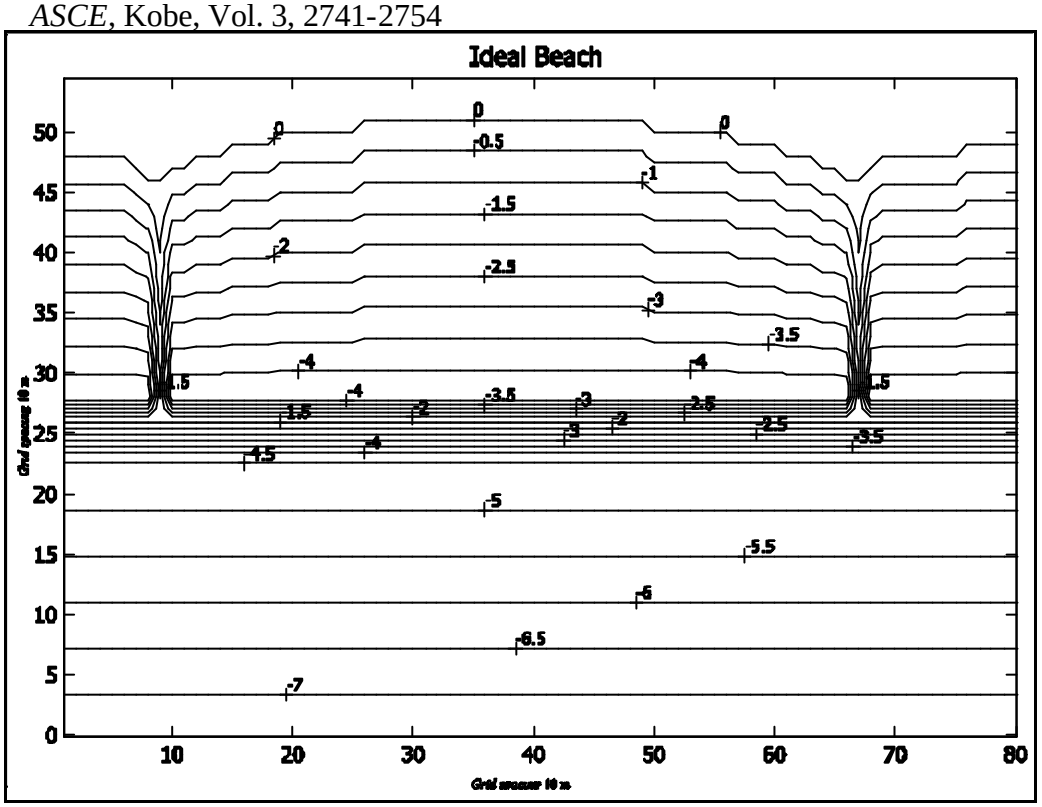

Figure 1: Contour lines of ideal beach [m]

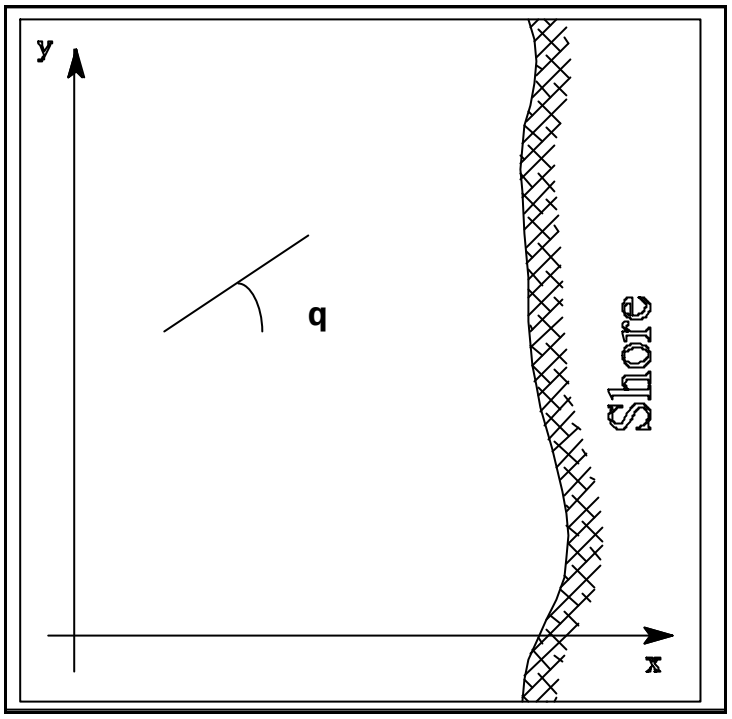

Figure 2: Cartesian axis definition

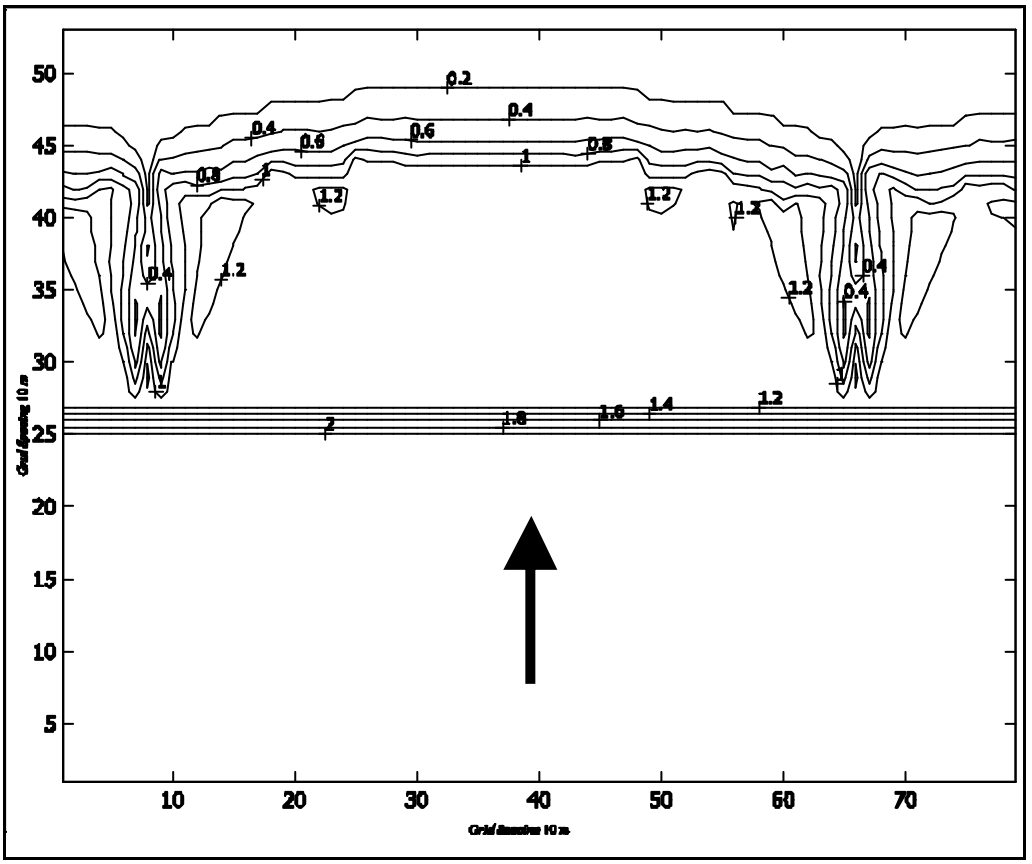

Figure 3: Contour lines of wave height distribution [m] for test A

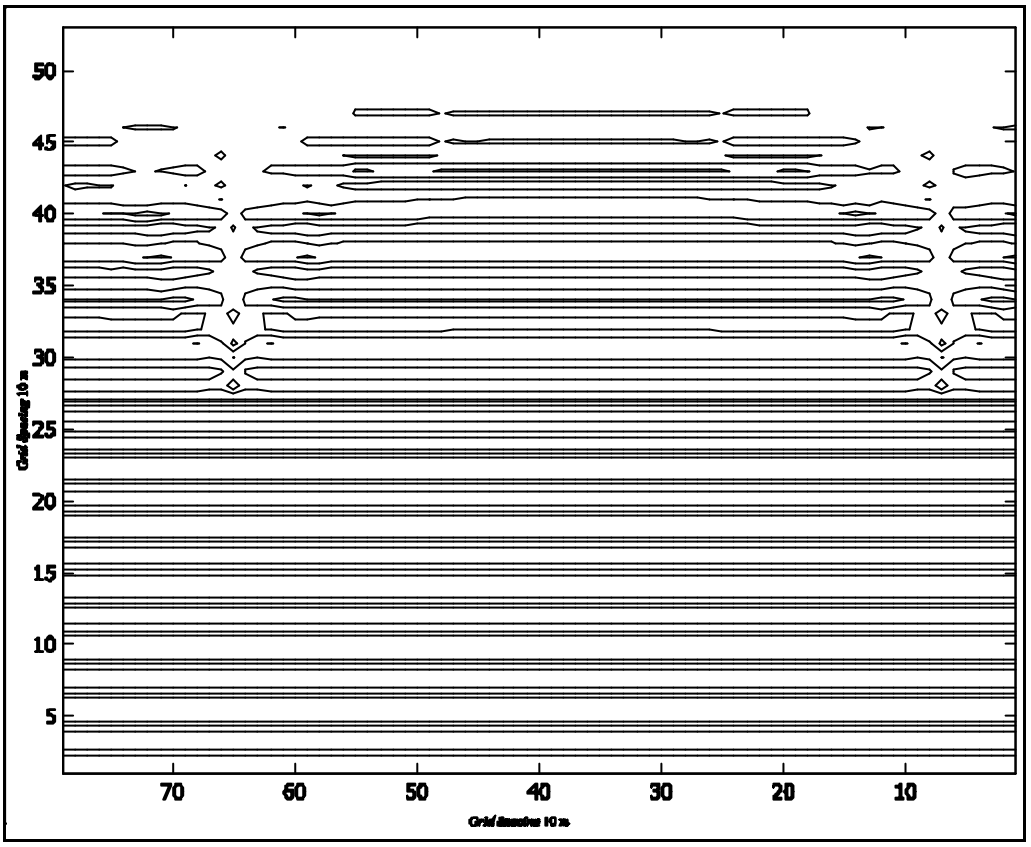

Figure 4: Contour lines of instantaneous surface displacement from still level water for test A

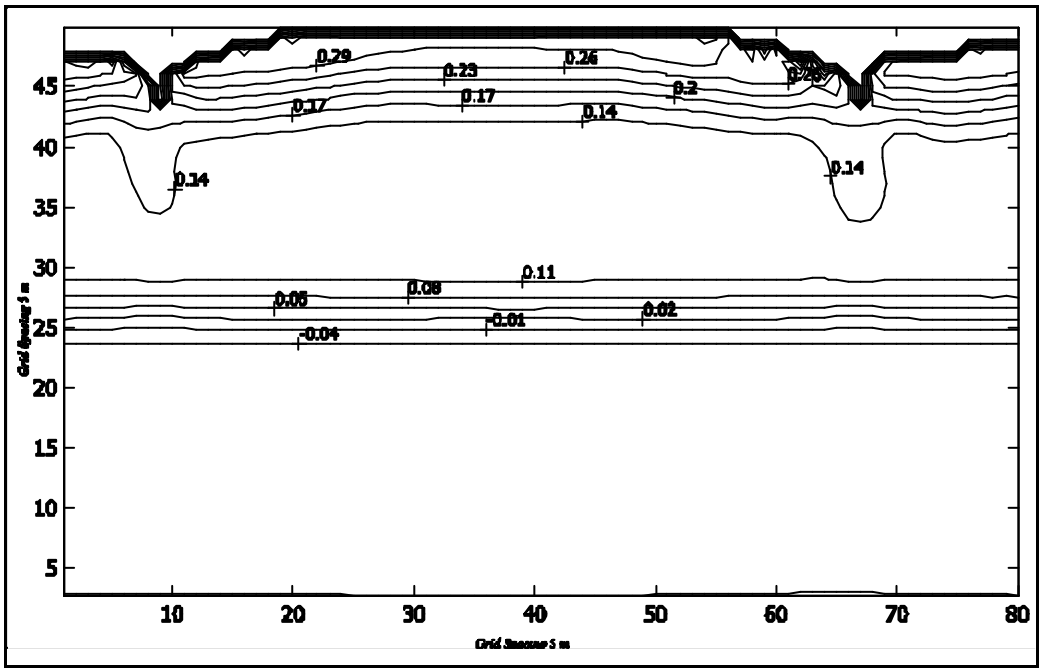

Figure 5: Contour lines of Mean water level [m] for test A

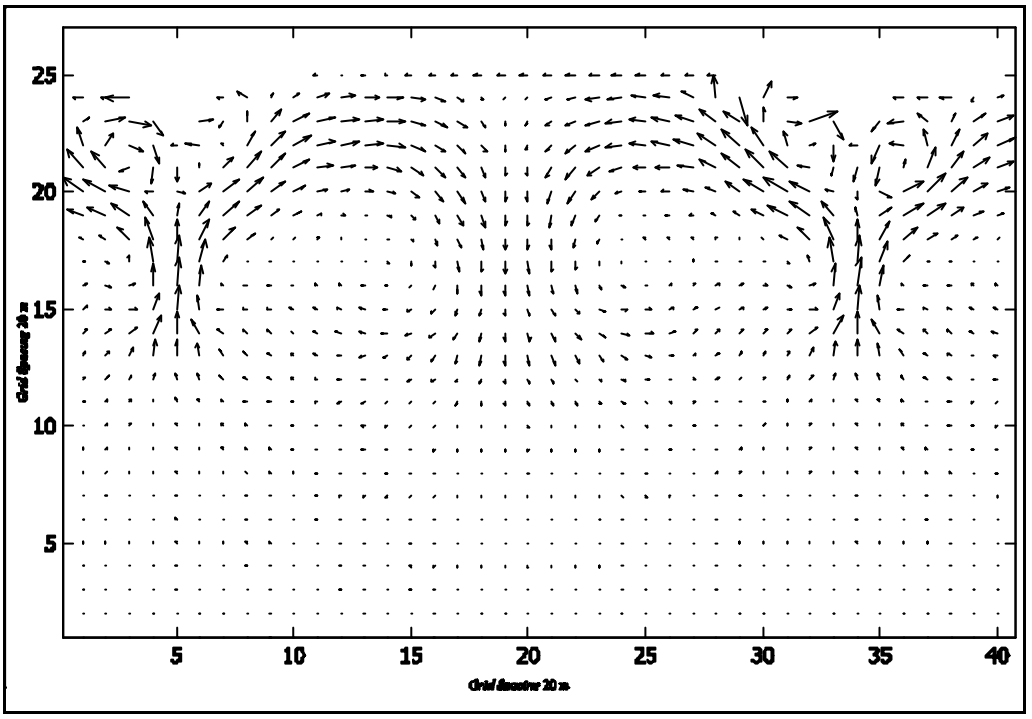

Figure 6: Velocity pattern for the test A

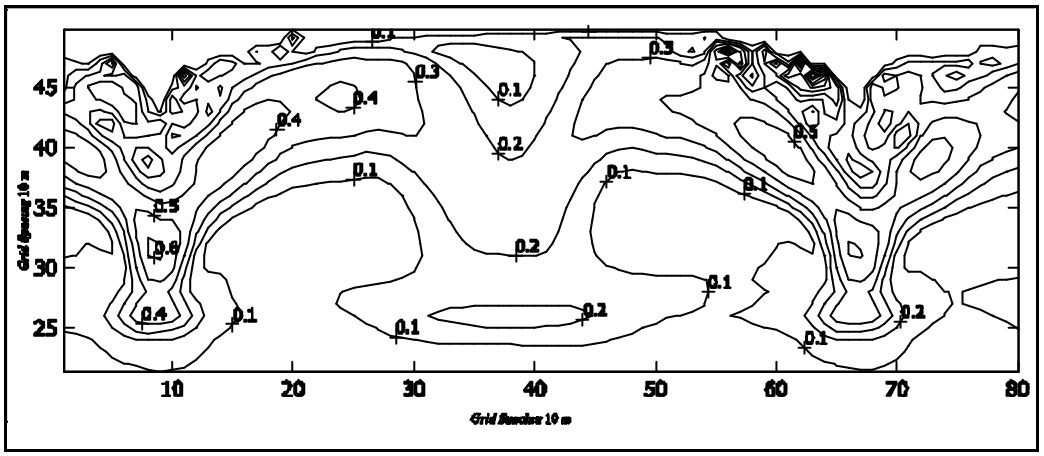

Figure 7: Contour lines of mean wave induced current velocity intensity [m/s] for test A

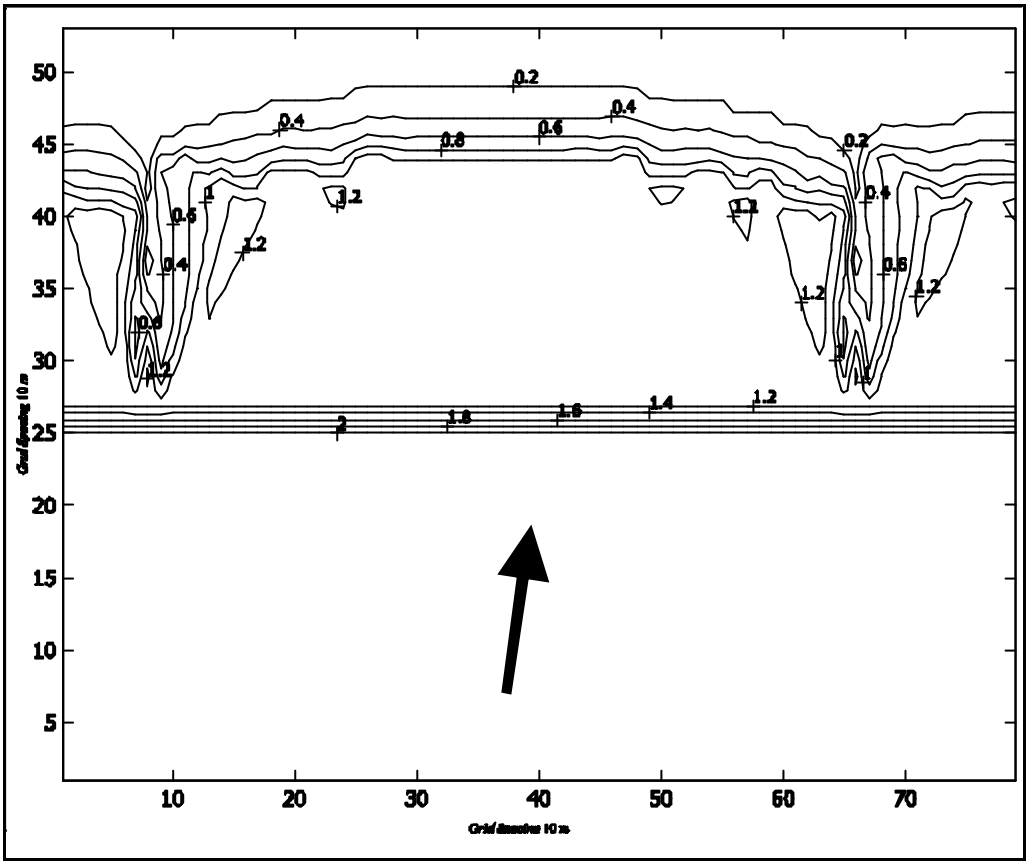

Figure 8: Contour lines of wave height distribution [m] for test B

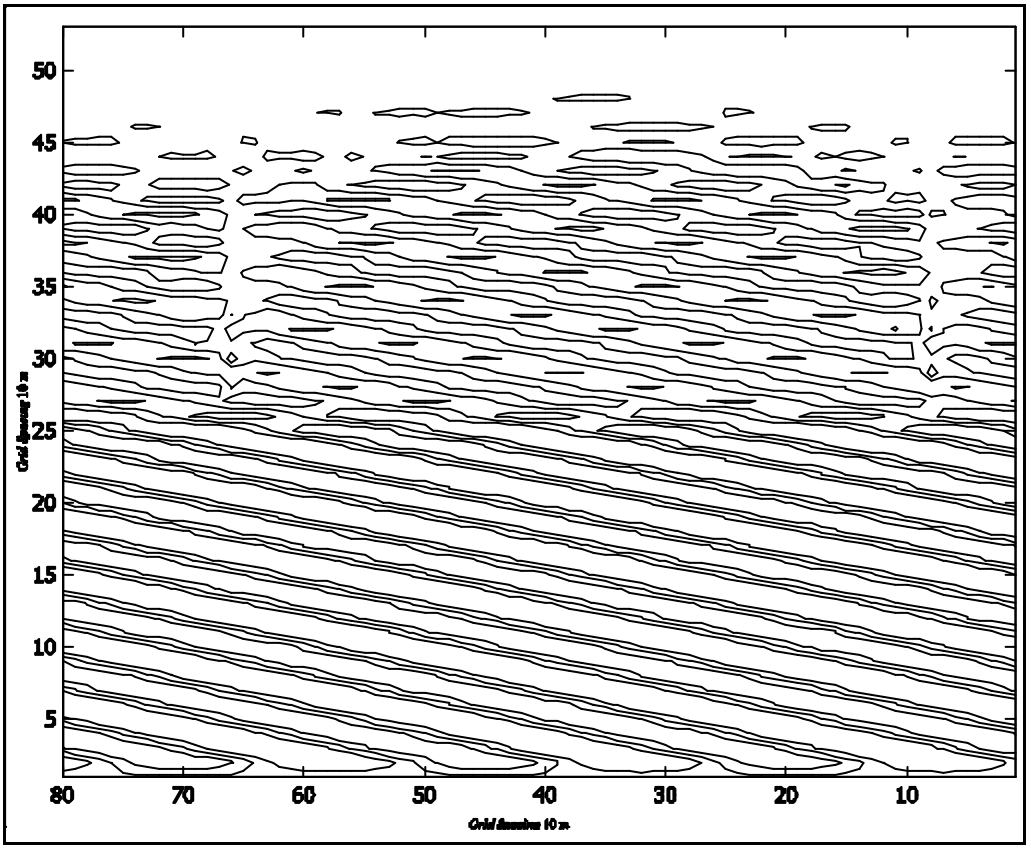

Figure 9: Contour lines of instantaneous surface displacement from still level water for test B

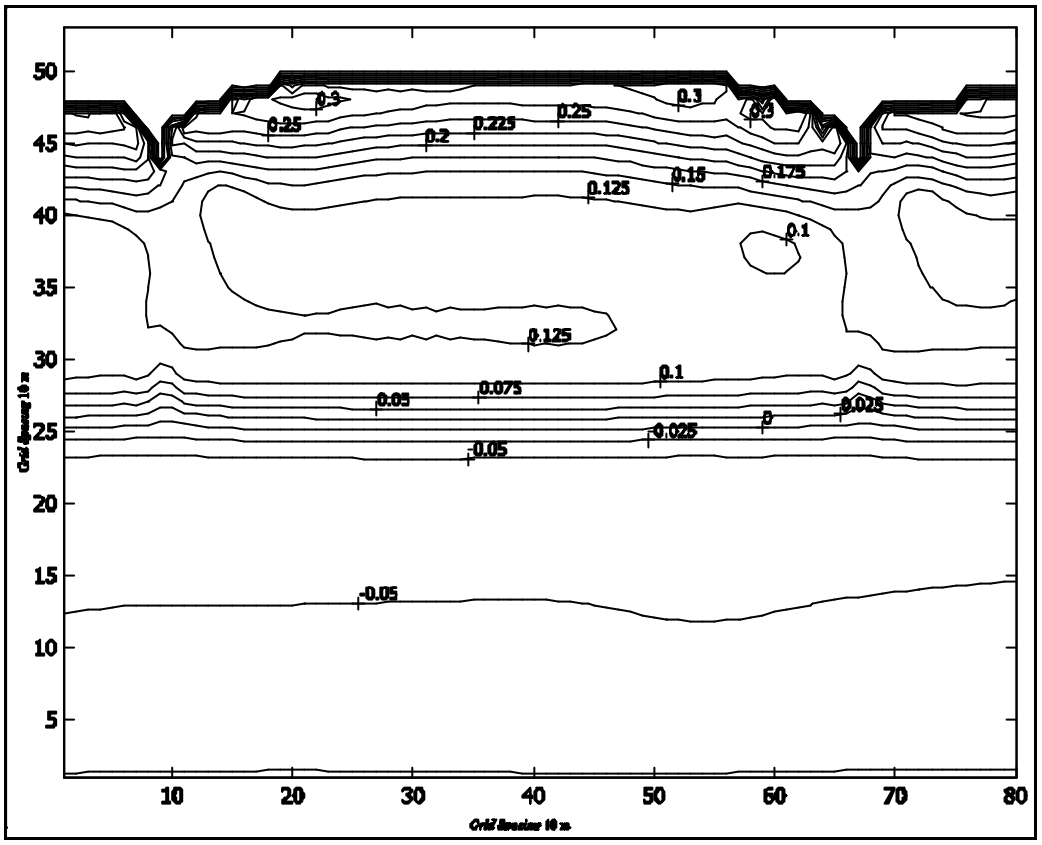

Figure 10: Contour lines of Mean water level [m] for test B

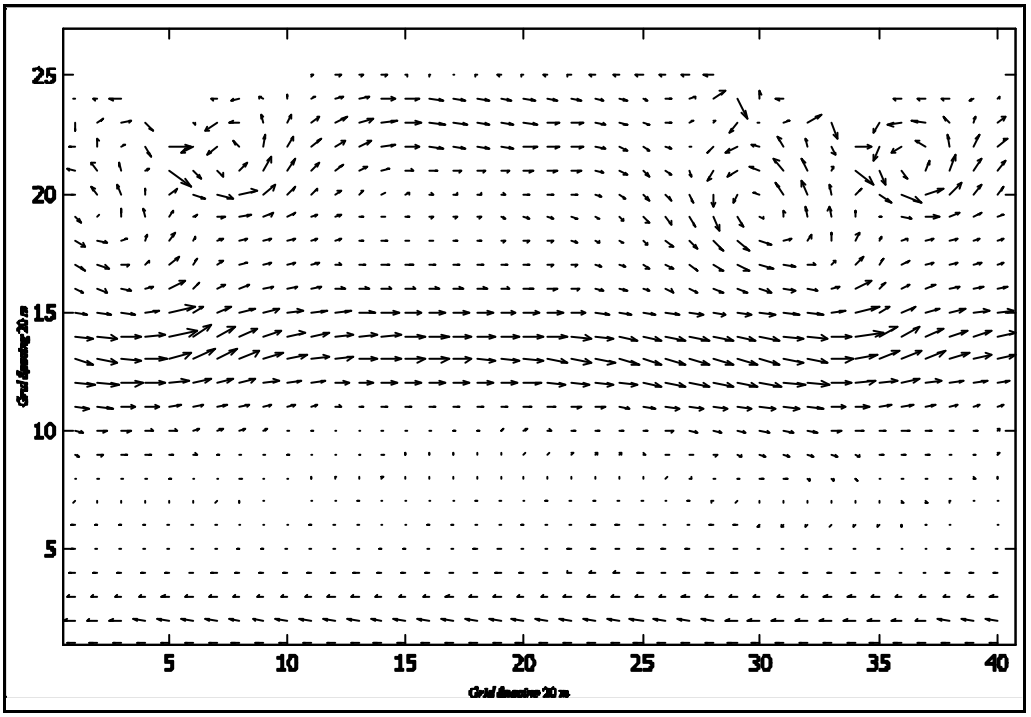

Figure 11: Velocity pattern for test B

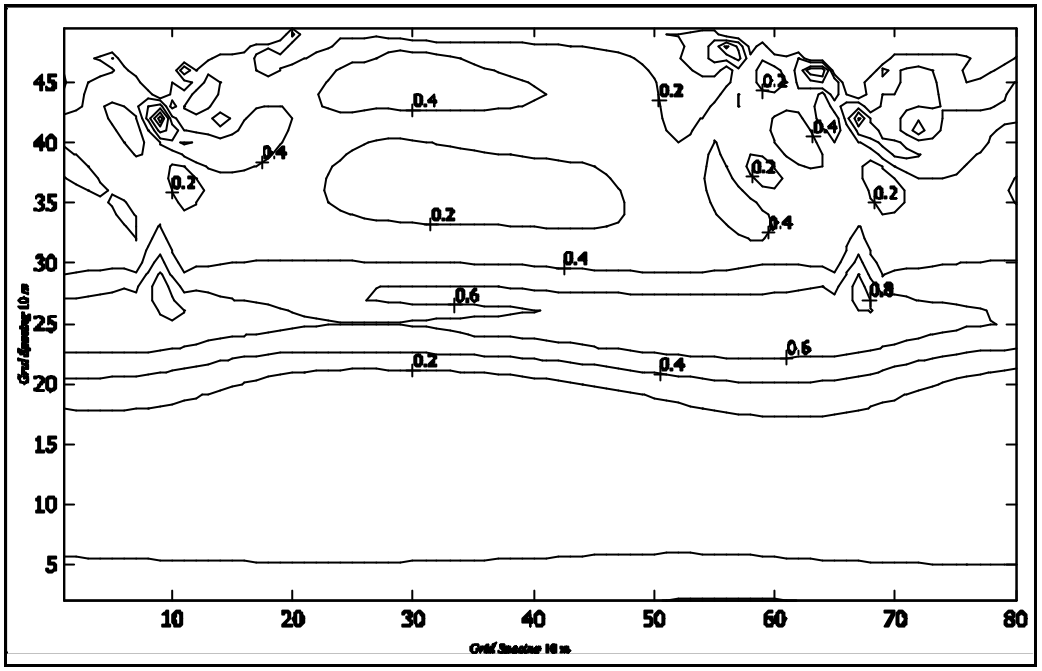

Figure 12: Contour lines of mean wave induced current velocity intensity [m/s] for test B

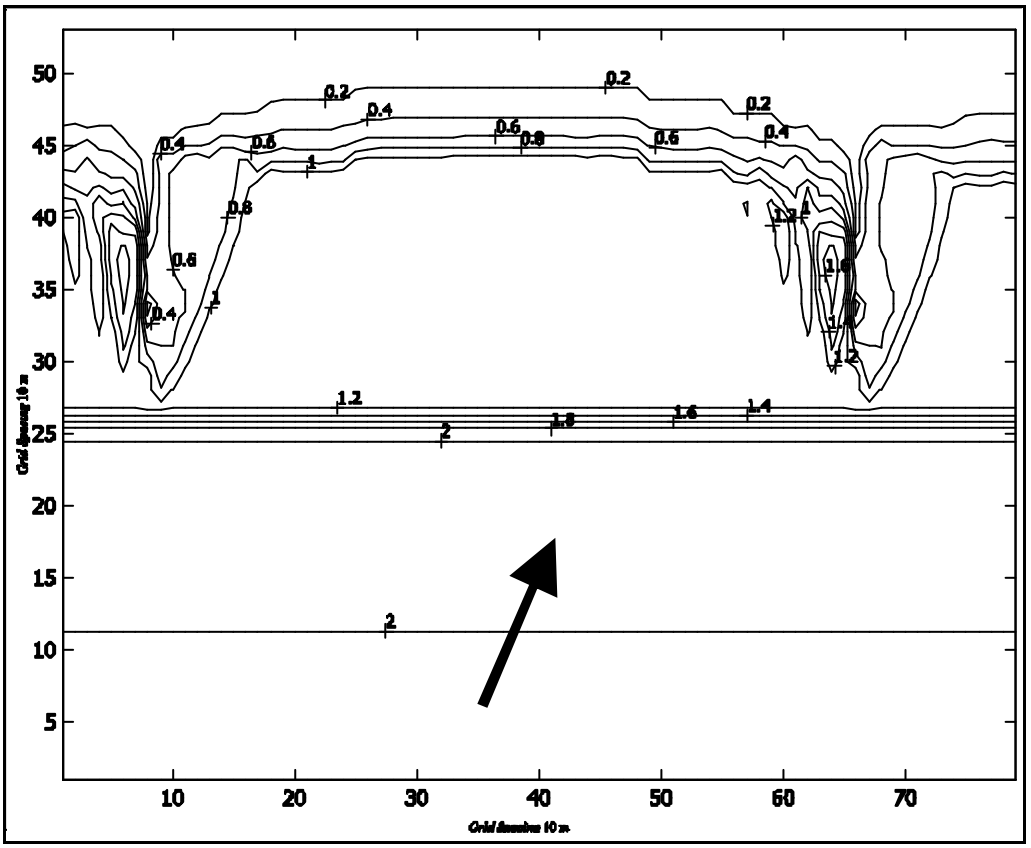

Figure 13: Contour lines of wave height distribution [m] for test C

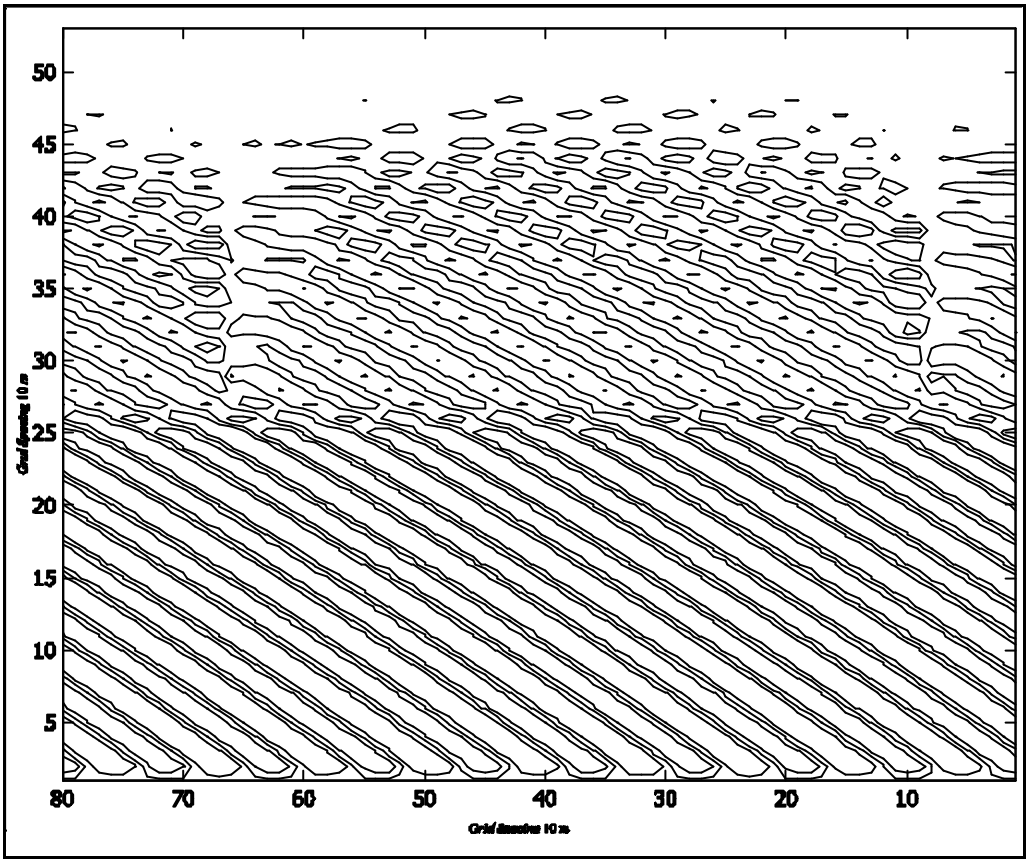

Figure 14: Contour lines of instantaneous surface displacement from still level water for test

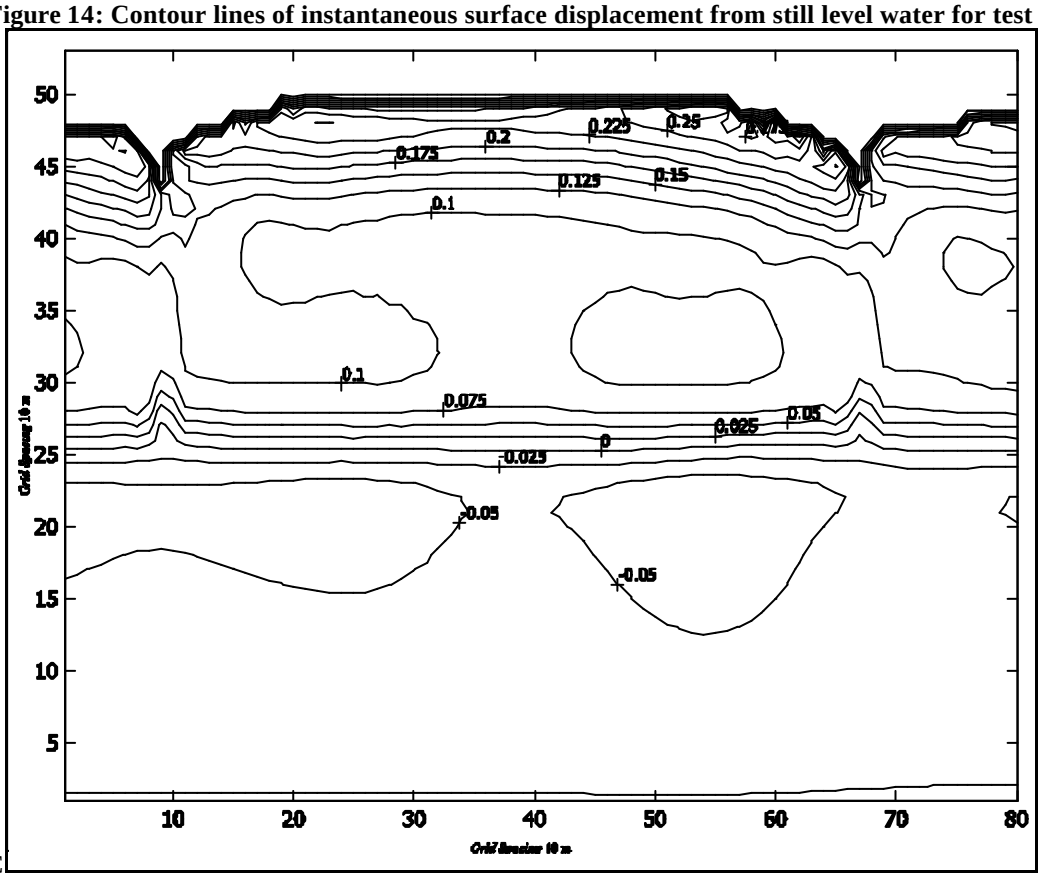

C

Figure 15: Contour lines of Mean water level [m]

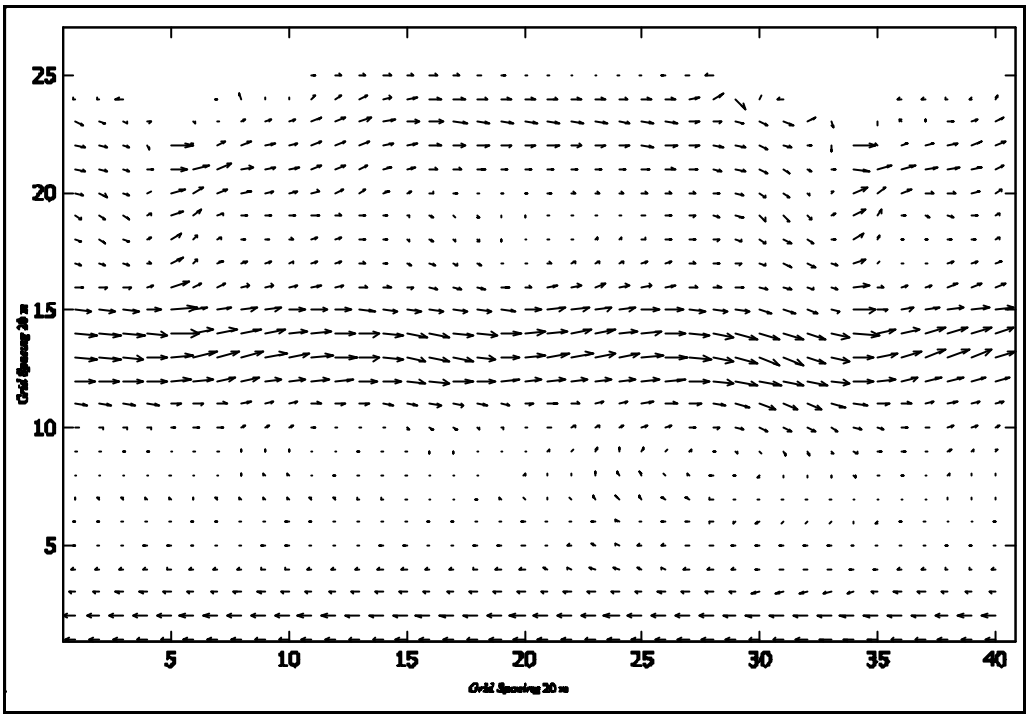

Figure 16: Velocity pattern for test C

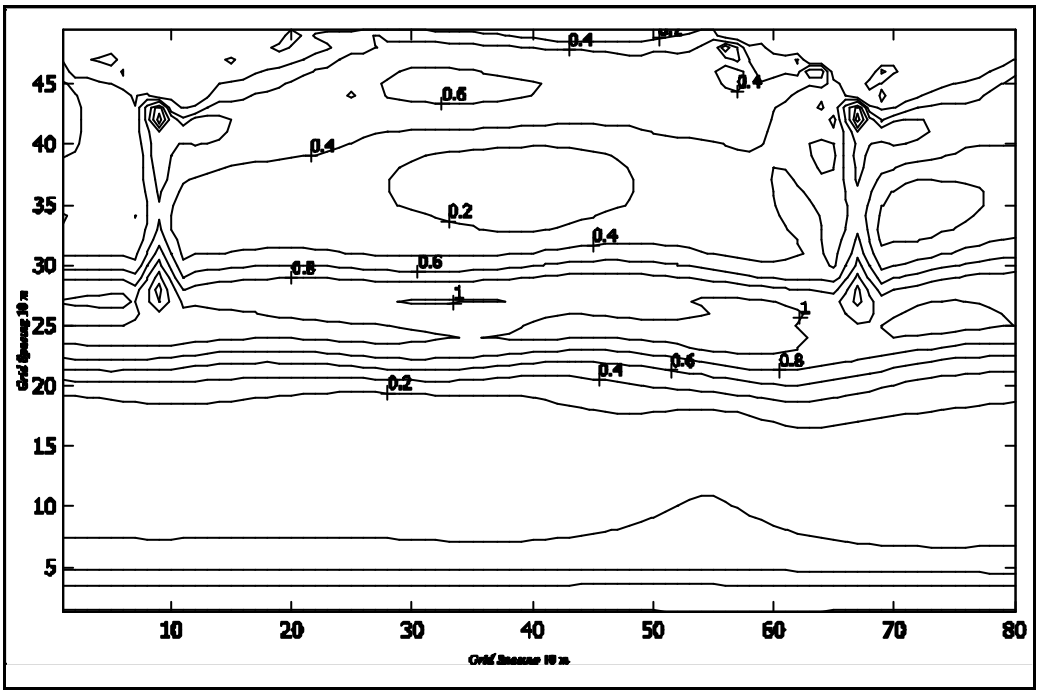

Figure 17: Contour lines of mean wave induced current velocity intensity [m/s] for test C

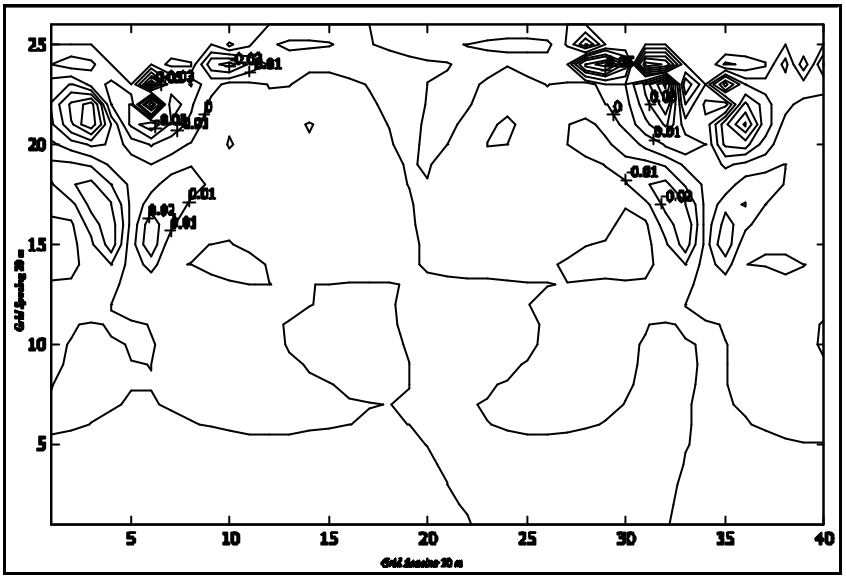

Figure 18: Contour lines of vorticity distribution for test A

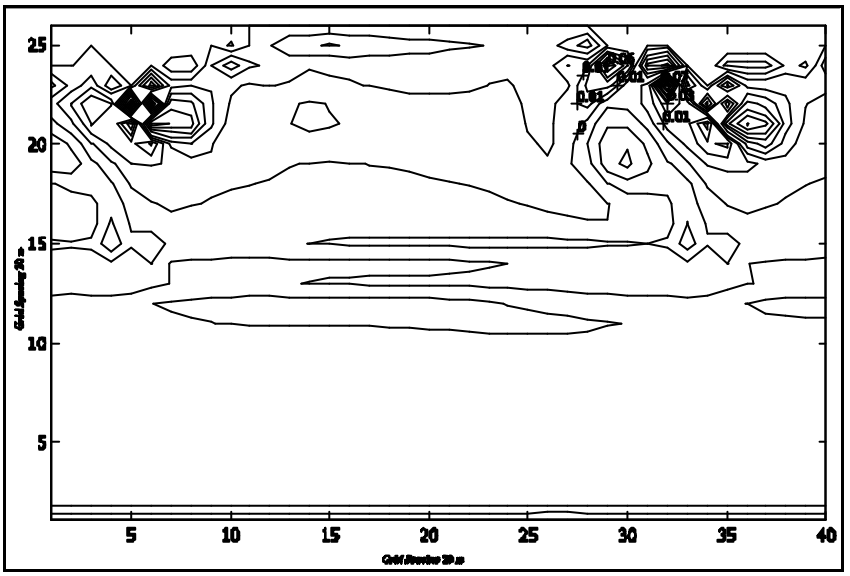

Figure 18: Contour lines of vorticity distribution for test B

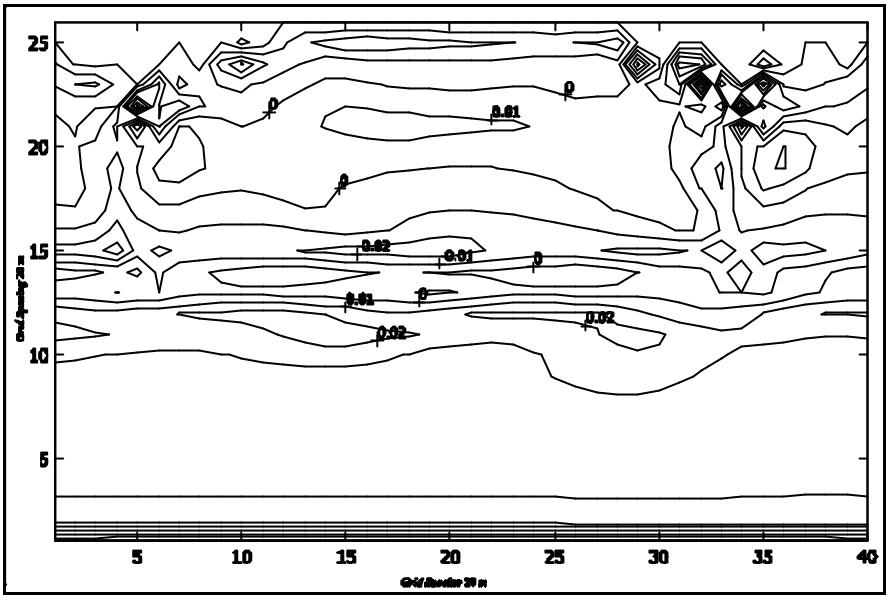

Figure 19: Contour lines of vorticity distribution for test C

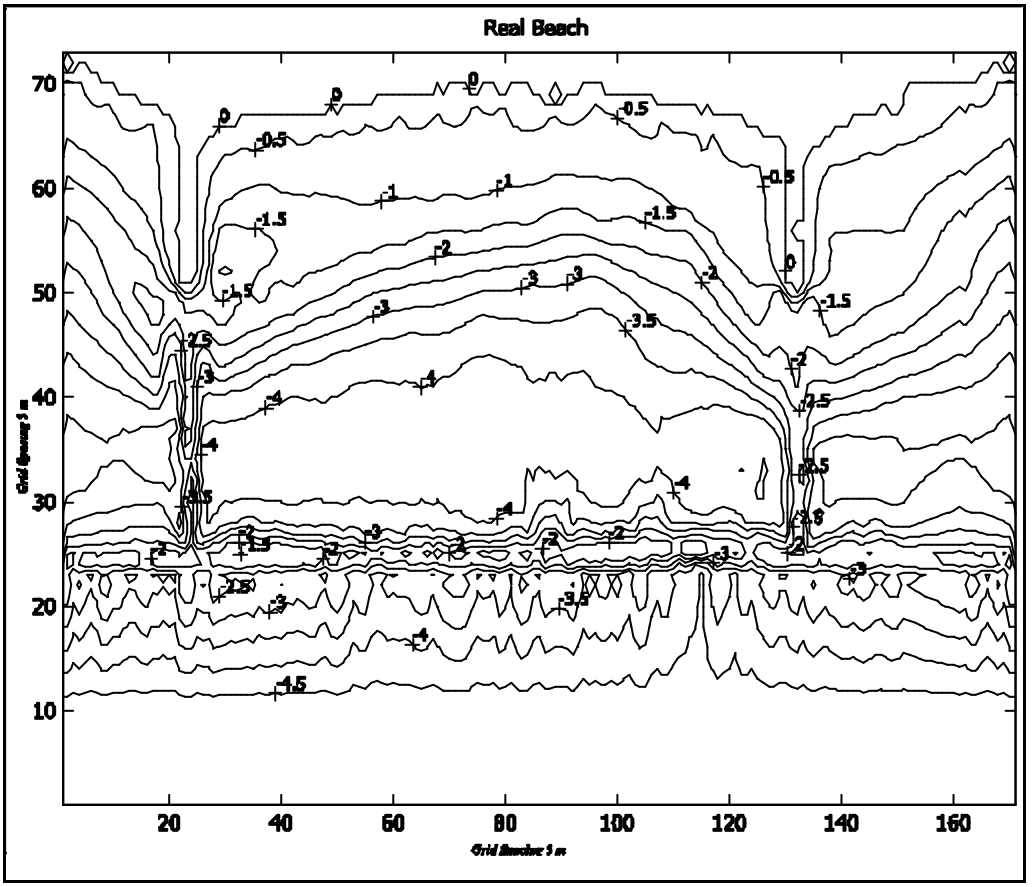

Figure 20: Contour lines of real beach based on March 1999 survey [m]

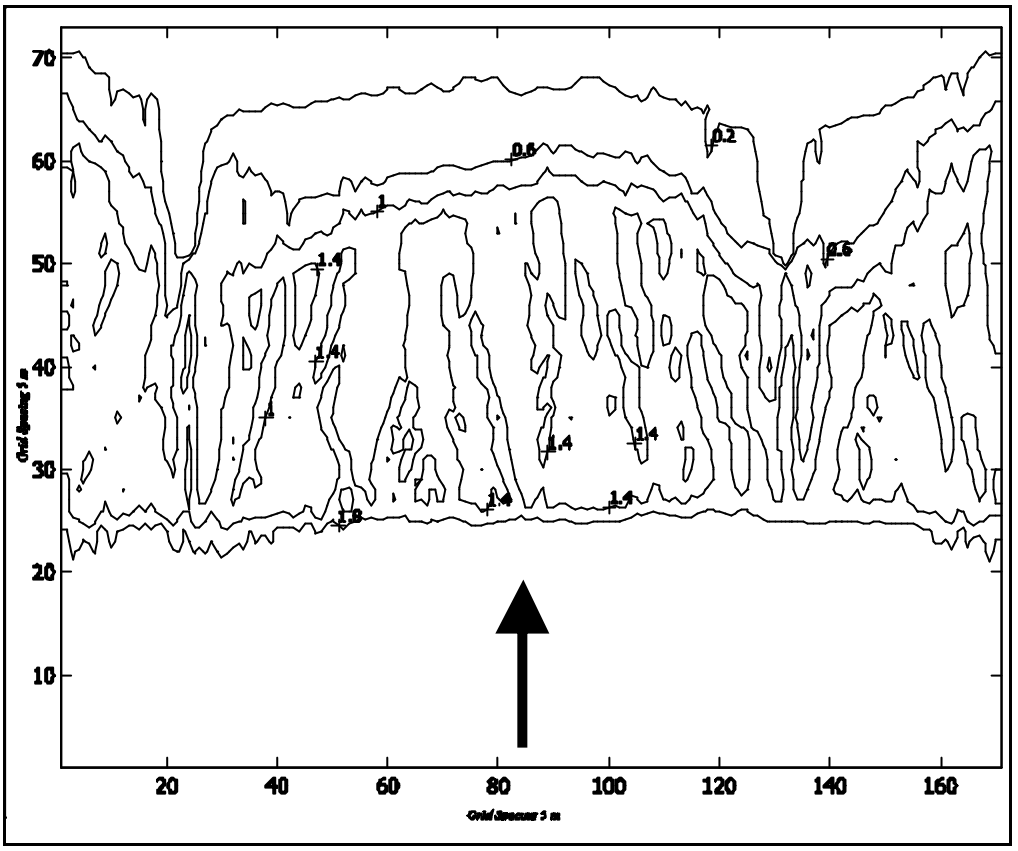

Figure 21: Contour lines of wave height distribution [m] for test D

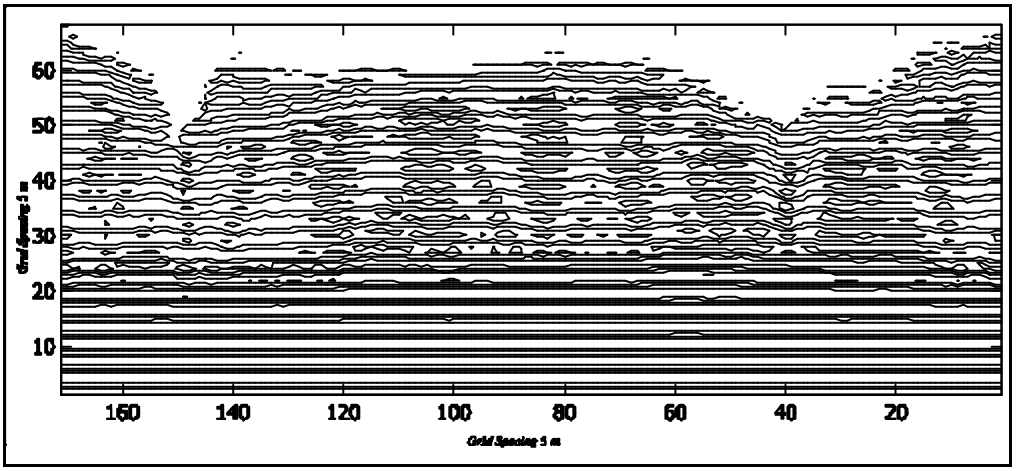

Figure 22: Contour lines of instantaneous surface displacement from still level water for test D

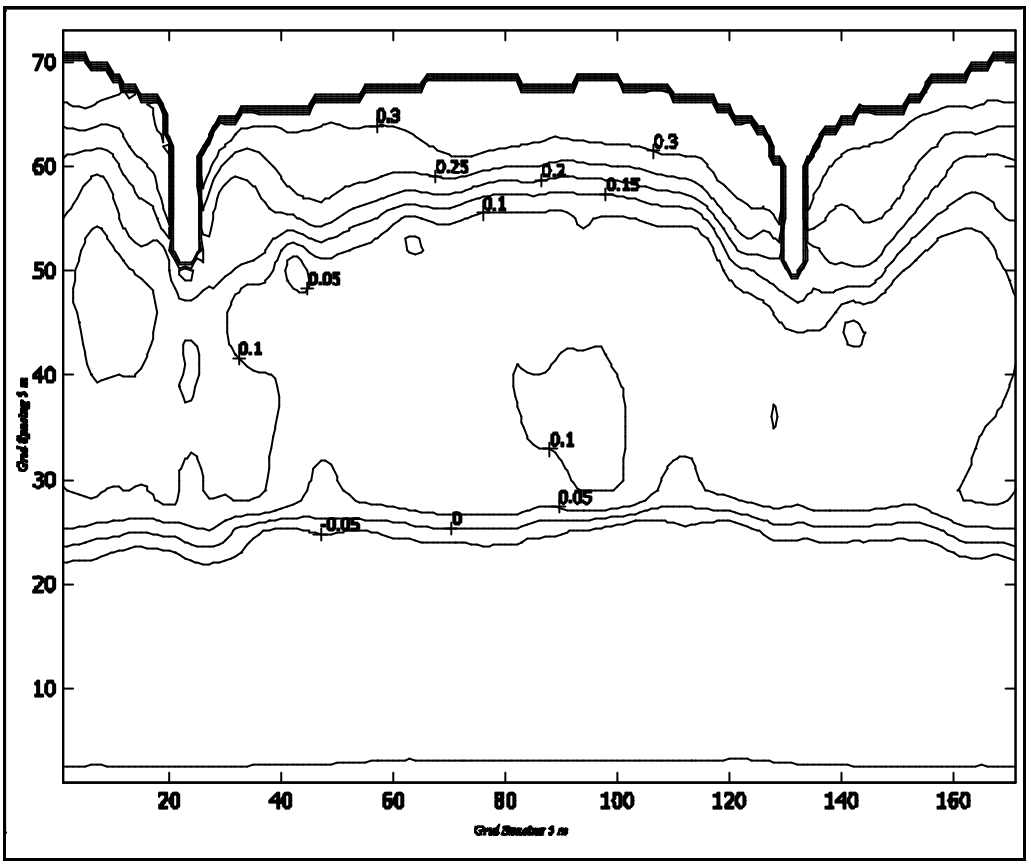

Figure 23: Contour lines of Mean water level [m] for test D

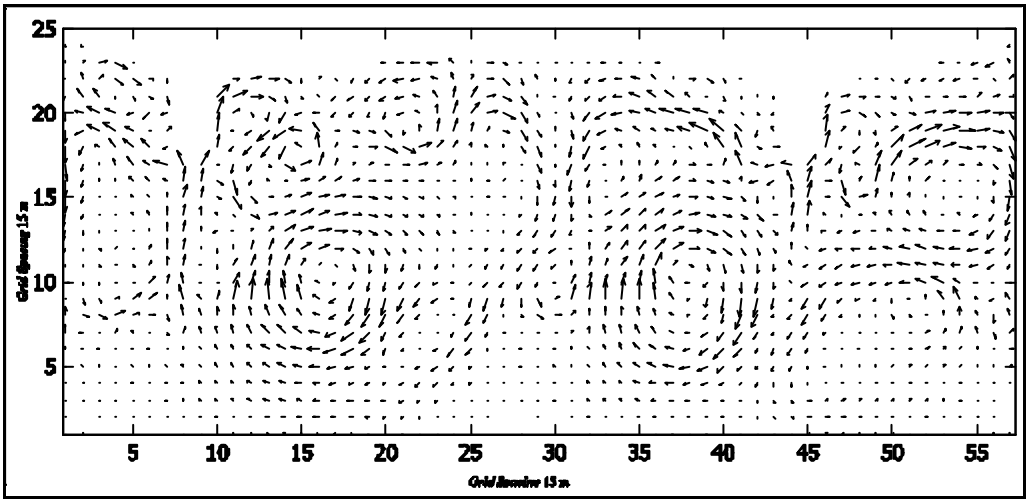

Figure 24: Velocity pattern for test D

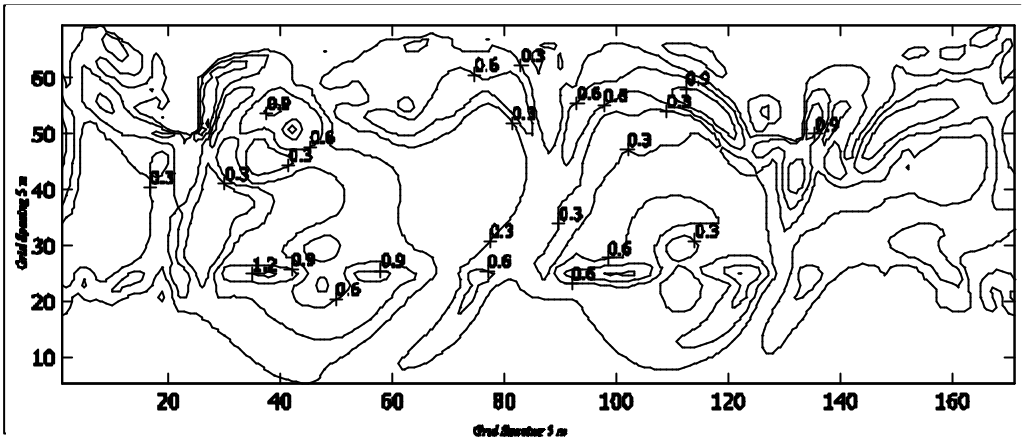

Figure 25: Contour lines of mean wave induced current velocity intensity [m/s] for test D

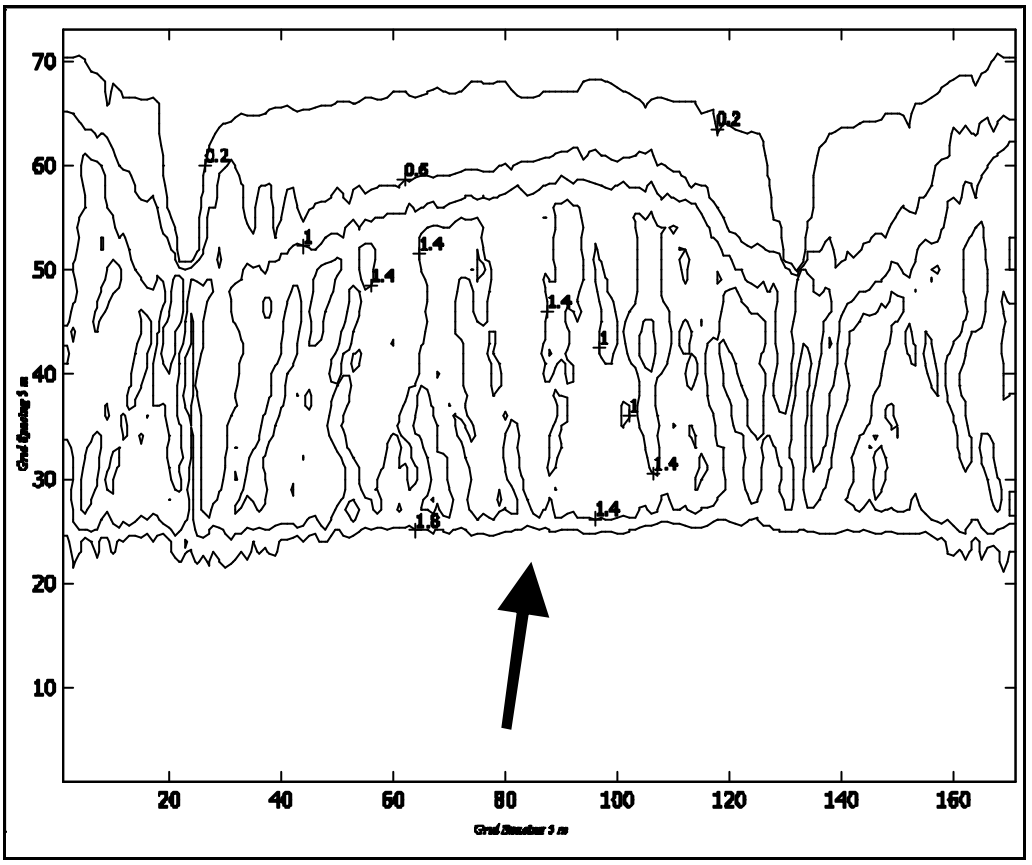

Figure 26: Contour lines of wave height distribution [m] for test E

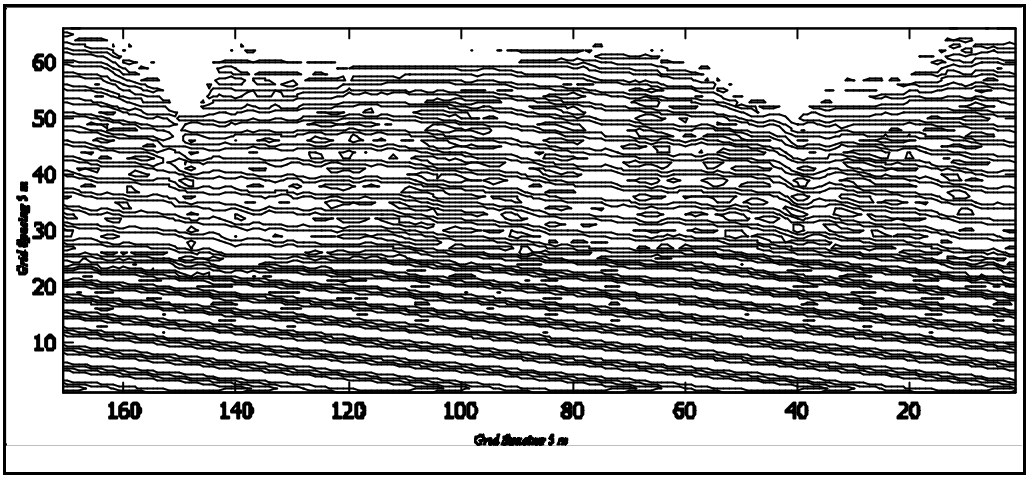

Figure 27: Contour lines of instantaneous surface displacement from still level water for test E

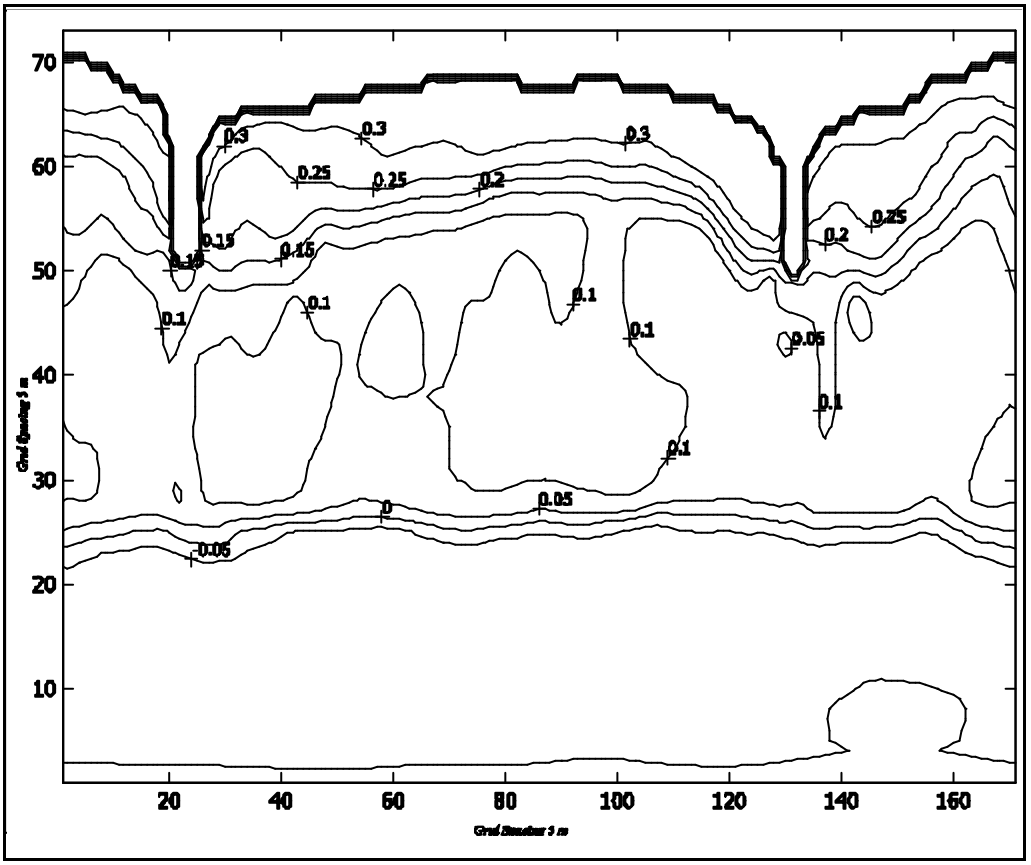

Figure 28: Contour lines of Mean water level [m] for test E

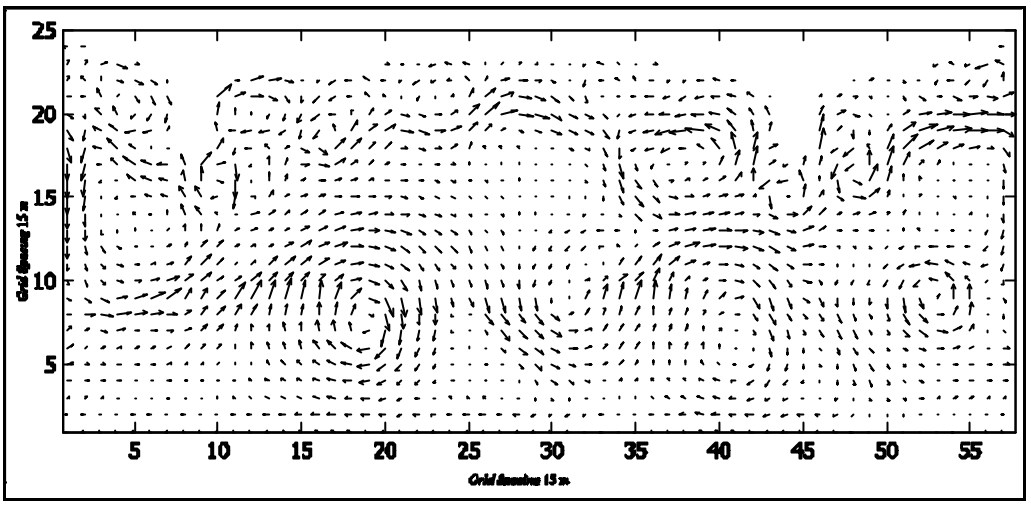

Figure 29: Velocity pattern for test E

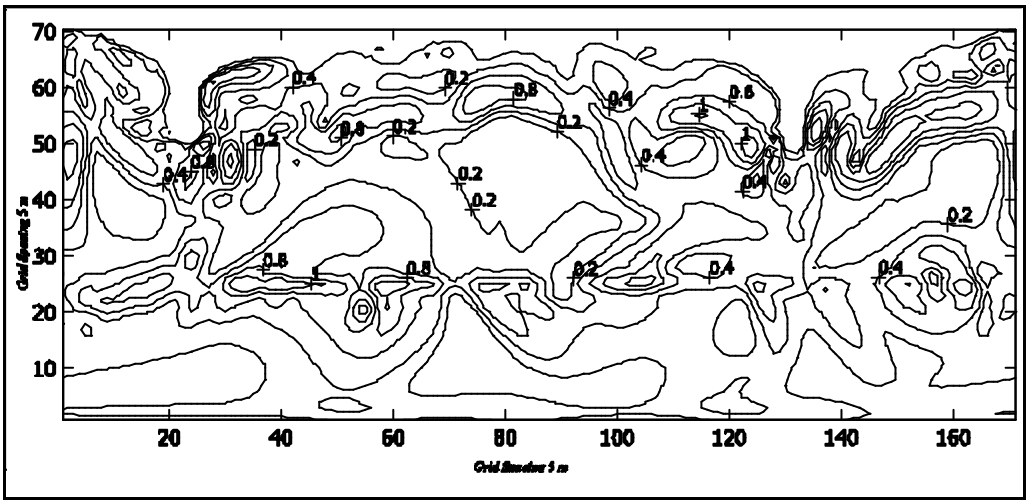

Figure 30: Contour lines of mean wave induced current velocity intensity [m/s] for test E

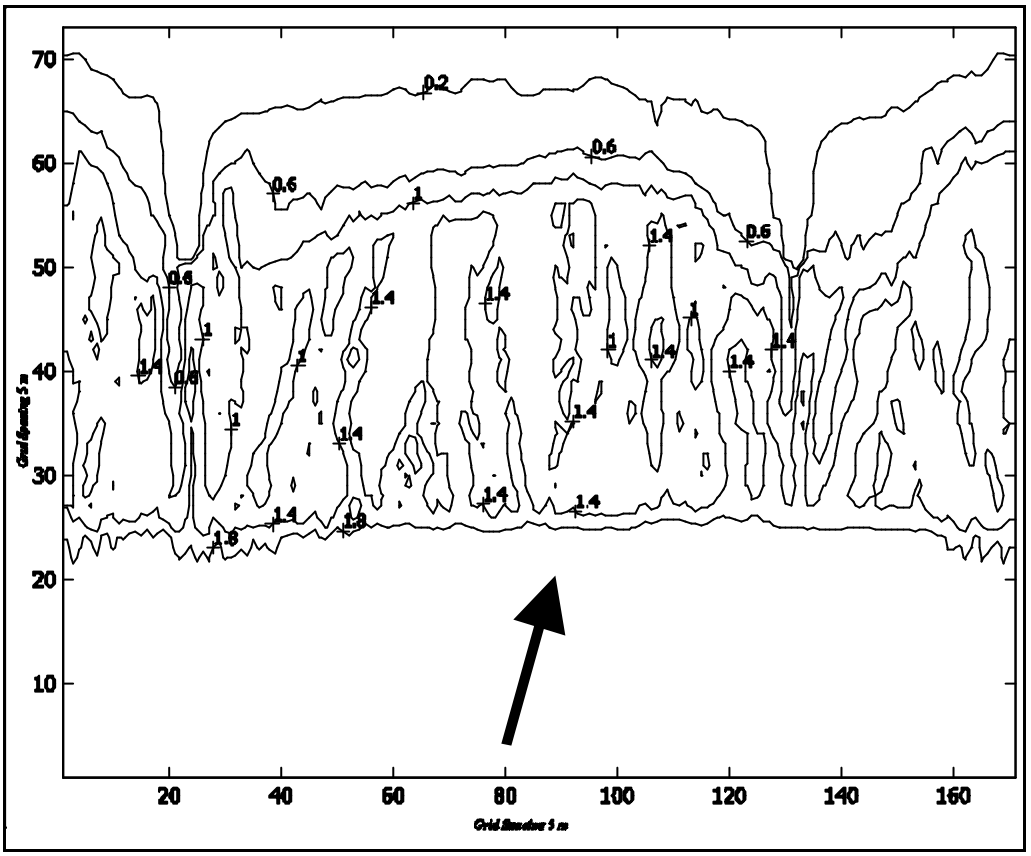

Figure 31: Contour lines of wave height distribution [m] for test F

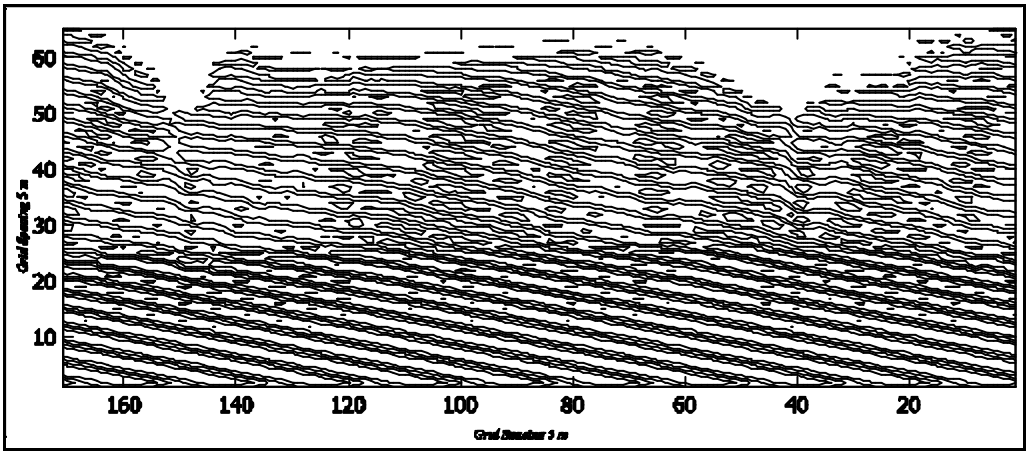

Figure 32: Contour lines of instantaneous surface displacement from still level water for test F

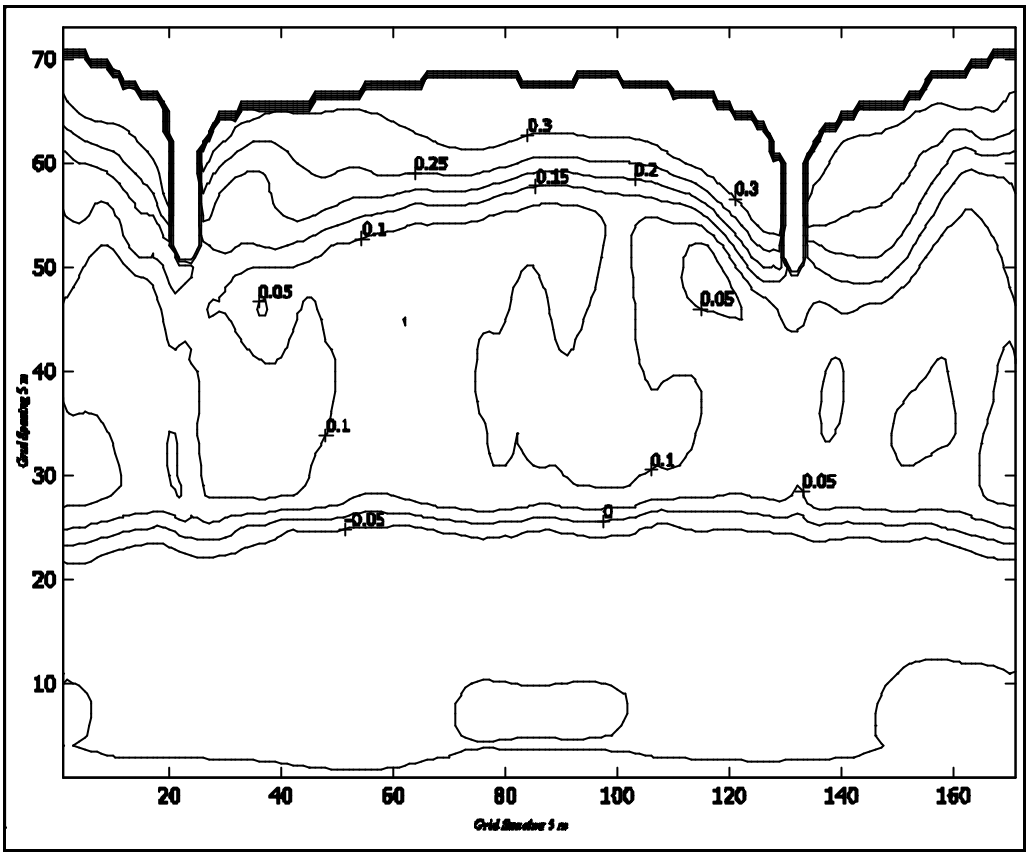

Figure 33: Contour lines of Mean water level [m] for test F

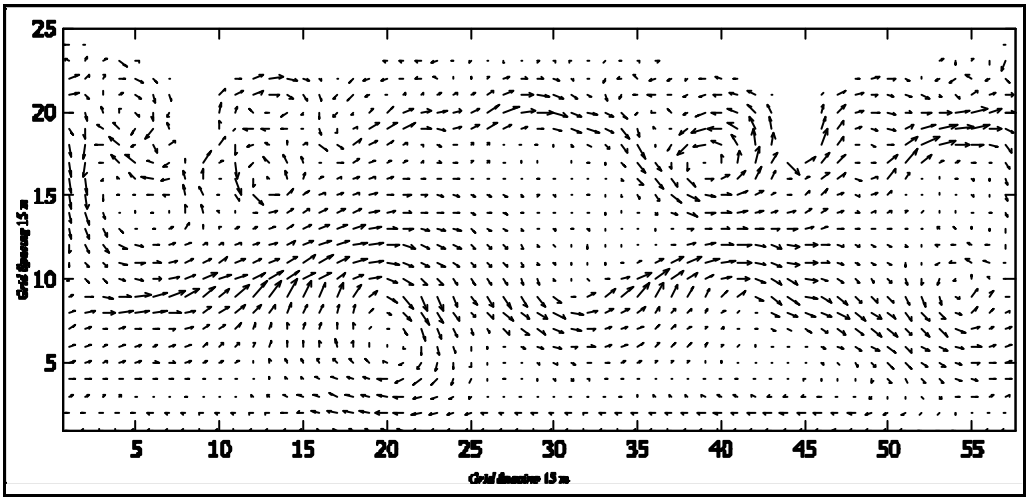

Figure 34: Velocity pattern for test F

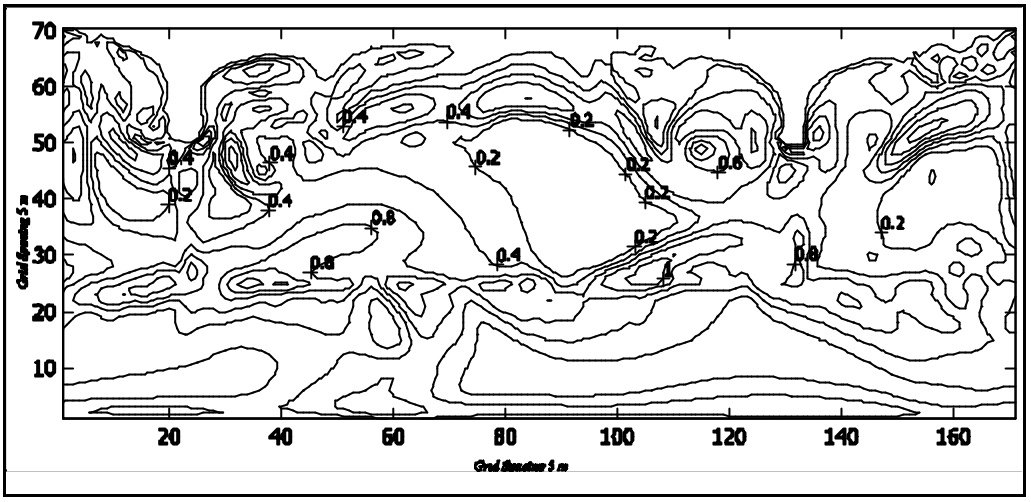

Figure 35: Contour lines of mean wave induced current velocity intensity [m/s] for test F

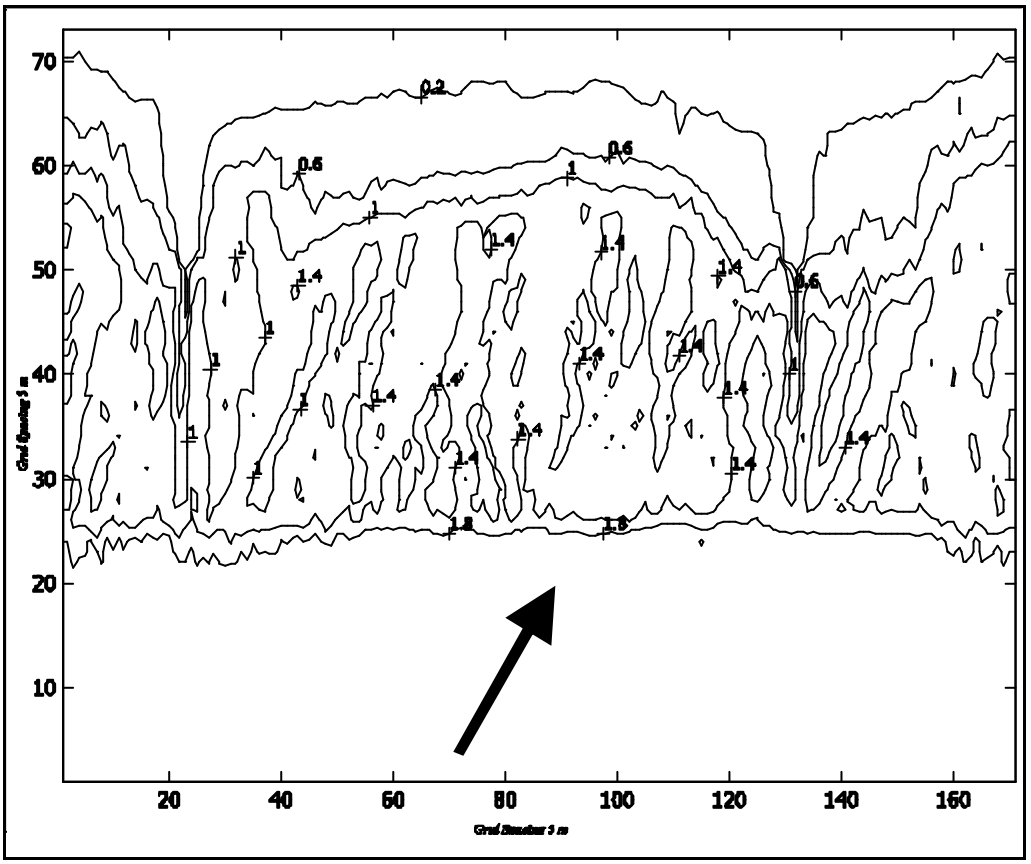

Figure 36: Contour lines of wave height distribution [m] for test G

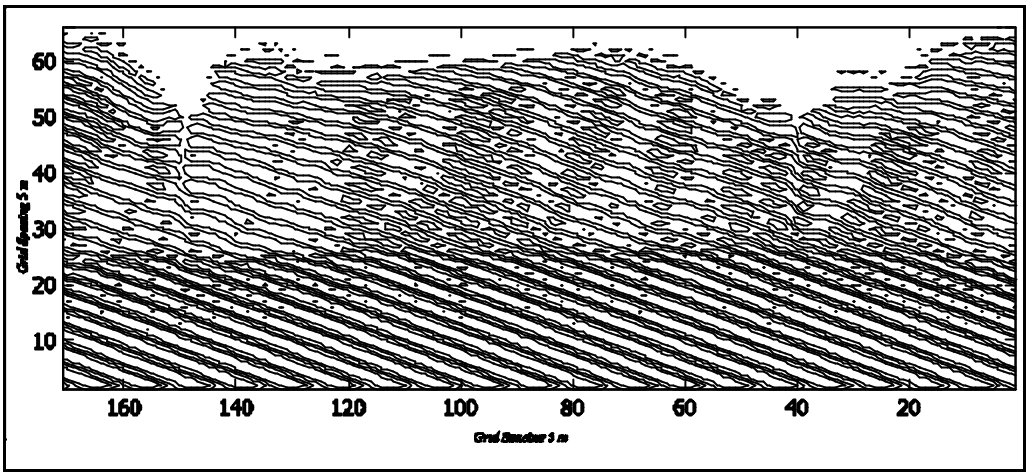

Figure 37: Contour lines of instantaneous surface displacement from still level water for test G

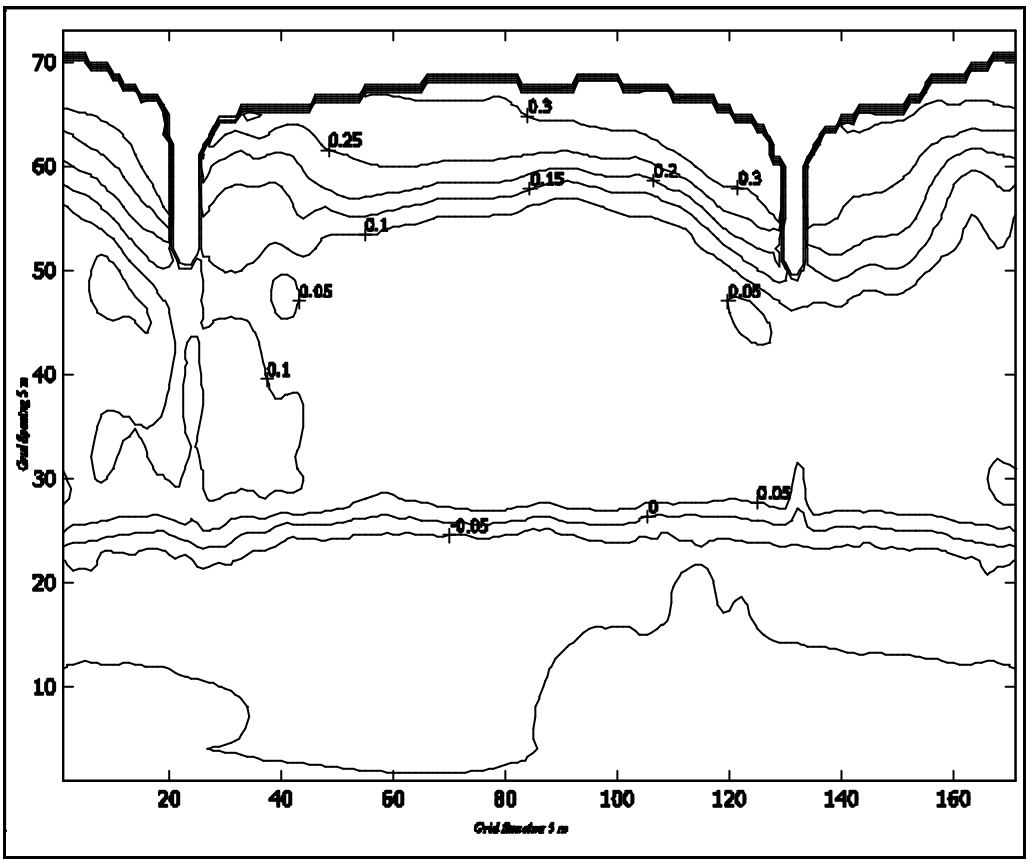

Figure 38: Contour lines of Mean water level [m] for test G

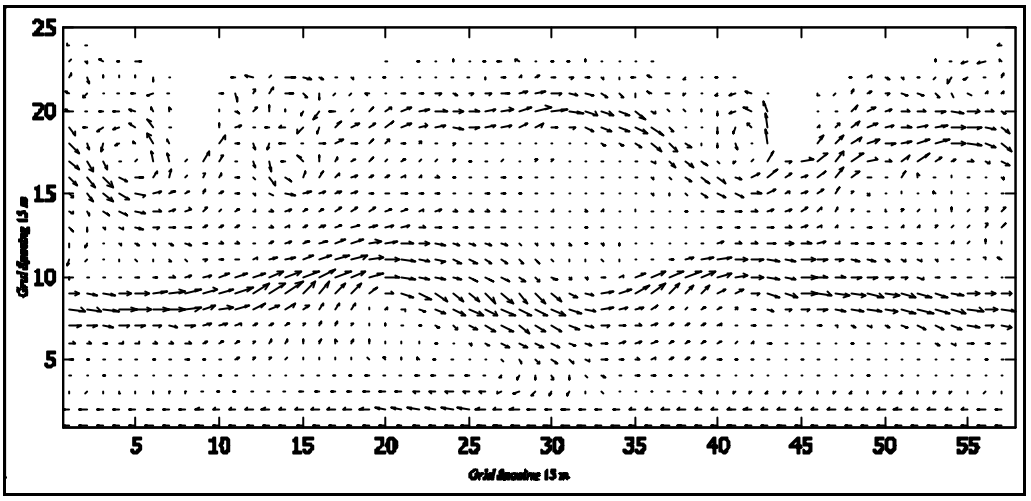

Figure 39: Velocity pattern for test G

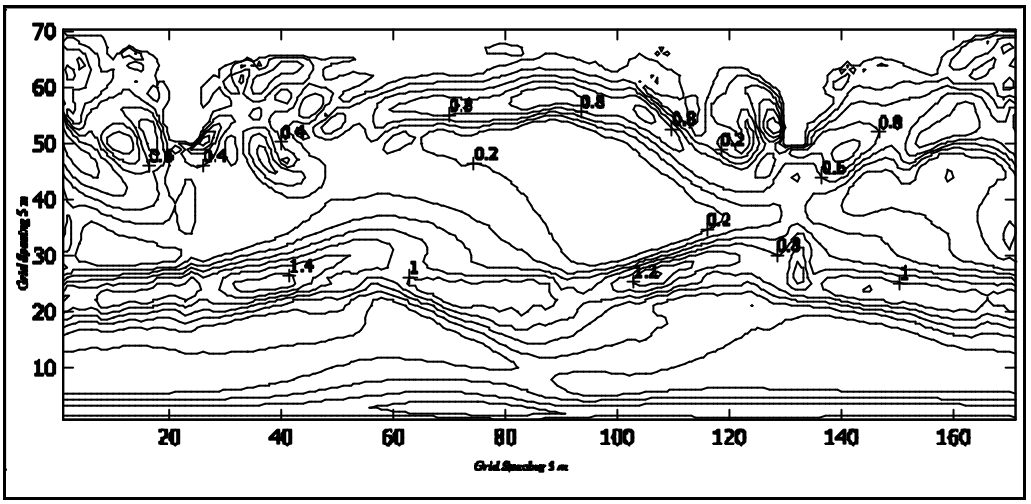

Figure 40: Contour lines of mean wave induced current velocity intensity for test G

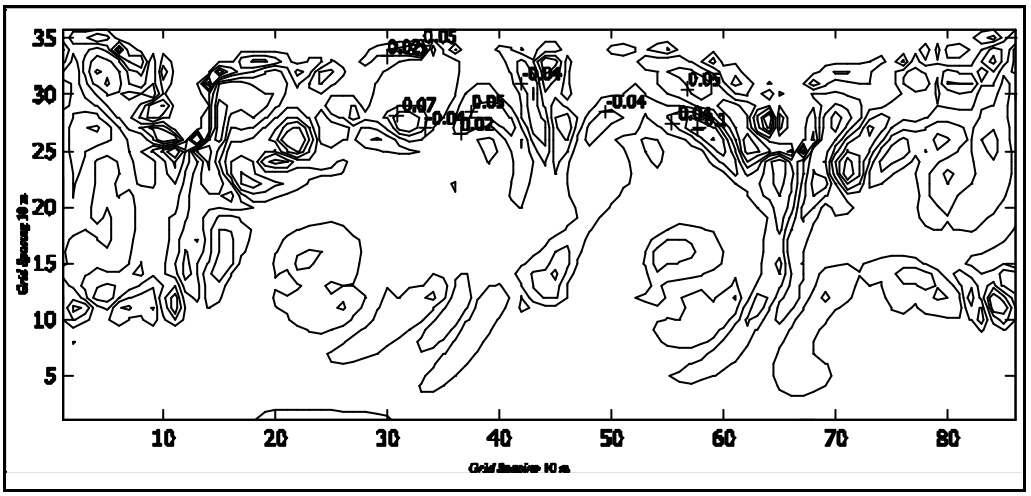

Figure 41: Contour lines of vorticity distribution for test D

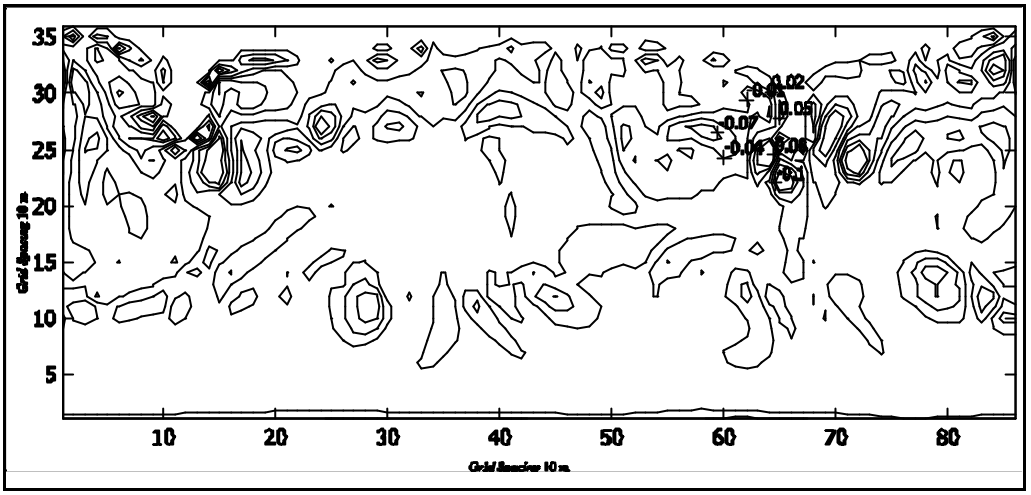

Figure 42: Contour lines of vorticity distribution for test E

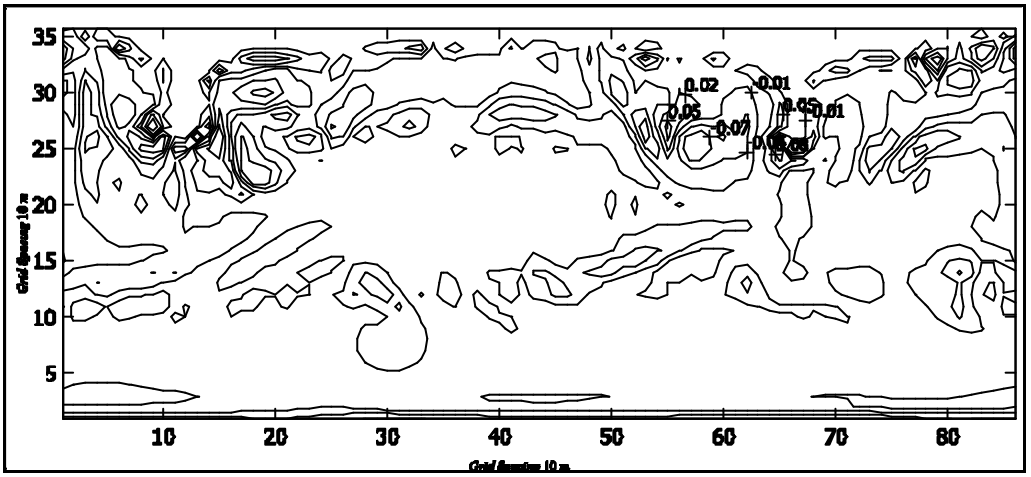

Figure 43: Contour lines of vorticity distribution for test F

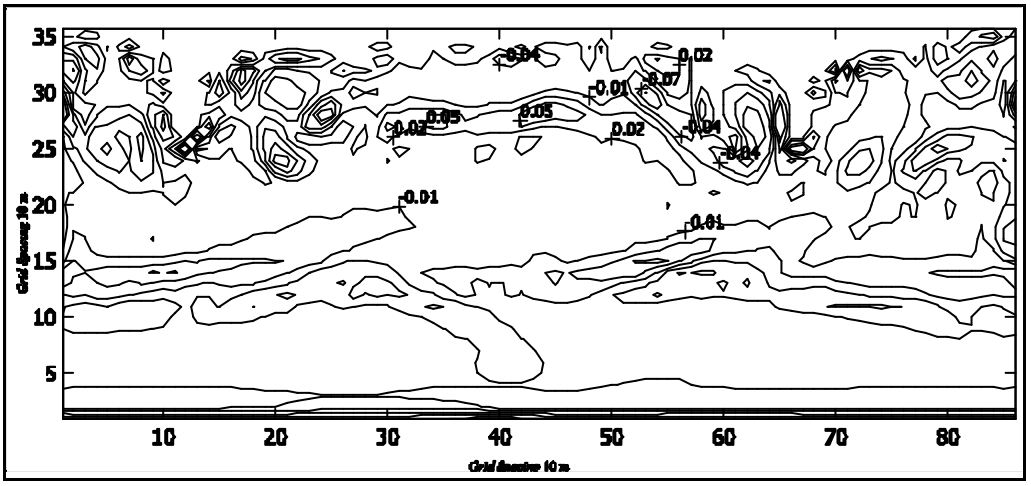

Figure 44: Contour lines of vorticity distribution for test G